Metallurgical Characterization and Performance of High Speed Steel Tool Materials used in Metal Cutting Applications

A thesis submitted in fulfilment of

the requirements for the degree of Masters by Research.

André Francis Rousseau

B. Eng (Mech) Hons, Swinburne University of Technology, 2001

School of Applied Sciences

College of Science, Engineering and Health

RMIT University

February 2016

Declaration

I certify that except where due acknowledgement has been made, the work is that of the author alone; the work has not been submitted previously, in whole or in part, to qualify for any other academic award; the content of the thesis/project is the result of work which has been carried out since the official commencement date of the approved research program; any editorial work, paid or unpaid, carried out by a third party is acknowledged; and, ethics procedures and guidelines have been followed.

André Francis Rousseau

Date of submission 22.02.2016

Acknowledgements

I would like to thank my supervisor Prof Derry Doyle for his patience in allowing me to learn and the wisdom to make it seem effortless. Derry is a wonderful colleague, ready to share and never left an idea un-discussed. Derry's enthusiasm for finding results was never ceasing and infectious. I would like to thank both Derry and Denise for inviting me into their family and sharing. I would like to thank my supervisor Prof Dougal McCulloch for his input to my work, consistency and humour and always politely laughing at my 'Dad' jokes. I will forever remember Dougal as always sat in his office working when most people had gone home. I would like to thank Dougal for his input into ideas and papers and his uncanny ability to cut to the chase when trying to publish a paper. I would like to thank my supervisor Dr James Partridge for his ever ending energy and enthusiasm and our discussion of science which inevitably would turn to England and the countryside around Bath. Wordsworth would be pleased.

I would like to thank the following people for all that they did;

- Peter Sutton for his continued support throughout the entire research programme.
- I would like to thank the CEO and board at Sutton Tools Pty. Ltd. for their continued support of the research undertaken.
- Dr Stephen Dowey for his input and support throughout the research programme.
- Defence Materials Technology Centre (DMTC).
- Jimmy Toton for the long discussions.
- Guy Stephens for his input and support.
- Phil Francis, Peter Rummel and Branco Cipreanu for all their help and advice with my research and of course the management and maintenance of the microscopy department.
- Edwin Mayes for his unending and uncomplaining input into our work.
- I would like to thank Masturina Kracica for her help in our paper and the endless discussions and her ability to make the corner of the research office a place of enjoyment.
- I would like to thank my legs for all their support.
- I would like to thank Zoran Lazarev for his mentoring and pragmatic approach to problems.
- Dr Yat Choy Wong for his continued support throughout my years at university.
- Hannah Golding for the long and inspiring conversations, the friendship and support.

I would like to thank my daughter Felicity Rousseau for accommodating my continued attendance at university. A good friend for life, no matter the time or distance apart. I would also like to thank my family for their support and nodding their heads at the appropriate intervals to signify they understood everything I prattled on about.

Author's Publications

Refereed Publications

1. **Vacuum heat treatment of high speed steel cutting tools,** International Heat Treatment & Surface Engineering, 2013. **7**(3): p. 110-114.
   A. Rousseau, E. Doyle, and D. McCulloch.

2. **Carbon Evolution during Vacuum Heat Treatment of High Speed Steel**
   Vacuum, 2016. **124**: p. 85-88.
   A.F. Rousseau, J.G. Partridge, Y.M. Gözükara, S. Gulizia, D.G. McCulloch.

3. **Microstructural and tribological characterisation of a nitriding/TiAlN PVD coating duplex treatment applied to M2 High Speed Steel tools**, Surface and Coatings Technology, 2015. **272**: p. 403-408.
   A.F. Rousseau, J.G. Partridge, E.L.H. Mayes, JT. Toton, M. Kracica, D.G. McCulloch, E.D. Doyle.

Abstract

The introduction of hard ceramic coatings has significantly improved the performance of high speed steel (HSS) cutting tools. However, failure mechanisms such as plastic deformation of the HSS substrate (beneath a ceramic coating) remain and motivate further research into vacuum heat treatment (VHT). This thesis describes investigations into the hardening response and carbon content of HSS before and after VHT. Poor hardening response of HSS was found to correlate with a loss of carbon in VHT. Full hardening response was achievable by removing surface oxide scale (predominantly Fe_2O_3 and Fe_3O_4) prior to VHT. Further investigation revealed an almost linear relationship between the surface oxide thickness pre-VHT and the post-VHT carbon content and hardening response. With surface oxide present, CO evolution and sample mass loss were observed during VHT of HSS above ~800 ℃. With the surface oxide removed, full hardening response was achieved and there was no measurable loss in carbon content post-VHT

To exploit the fully hardened HSS in a coated tool, plasma nitriding followed by steered cathodic arc evaporation TiAlN ceramic coating process was performed (with no break in vacuum) in an industrial scale deposition chamber. Bright plasma nitriding at ~480 ℃ resulted in a fracture tough diffusion zone with no evidence of a compound layer or grain boundary precipitation. M2 HSS coupons and M2 ¼-inch jobber drills were similarly tested microstructurally and mechanically in untreated, plasma-nitrided, coated-only and duplex. The ¼-inch jobber drills were subjected to accelerated drill testing into D2 tool steel which revealed a significant increase in cutting performance of the duplex treatment compared with un-treated tools. Electron microscopy of the sectioned tools indicated that this improved performance was due to increased toughness of the cutting edge coupled with an increase in adhesion at the substrate-TiAlN coating interface.

Table of Contents

List of figures

Chapter 1. Introduction and Literature review

1.1 Cutting tool market

The global cutting tool market, worth over $11 billion annually [1]. It is a market largely comprised of two classes of cutting tool materials, namely, high speed steel (HSS) and carbide. The latter is based on the cermet WC-Co and is produced by the powder metallurgy route. HSS is a complex alloy tool steel produced largely by the traditional casting and forging route although an increasing volume is produced by powder metallurgy. Both classes of tool materials have now been available to the tooling market for more than one hundred years [2]. In this period, developments in both of these tool materials has resulted in significant advances in structure and properties such that they are able to deliver high cost benefit performance and so meet the demands of modern manufacturing.

HSS is a complex alloyed tool steel that is recognised for its high hot hardness. Originally based on tungsten and later molybdenum and vanadium, HSS has a room temperature hardness of 850-900 HV. While HSS loses hardness above 600 ℃ carbide tools perform well up to around 700 ℃ however HSS has a higher toughness compared with carbide. To achieve good cutting performance from HSS, an appropriate hardening response must be provided in heat treatment [3, 4]. The aforementioned hot hardness means that HSS tools can cut at higher feeds and speeds when compared with earlier high carbon steel tools. This is due to the complex nature of precipitation hardening (also referred to as secondary hardening) in HSS. Nano-scale precipitated carbides occupy vacancies and dislocations during the tempering phase of the heat treatment process.

In addition to correct heat treatment of HSS for cutting tools, the HSS supply route must also be considered. Hot working the HSS billet can lead to chemical/structural modifications including surface oxide [5], carbide stringers [6] and micro-voids [7] from cold drawing. Cold drawing (high strain deformation), used to reduce ‘as received’ coil to desired size, has a reduction limit [8, 9] hence the need for sub-critical annealing between draws, with decarburization associated with this process [10]. Cold drawing can introduce vacancies [11] and residual stresses [12, 13]. HSS cutting tools include a typical twist drill Figure 1-1 (a) and a HSS orthogonal cutting tool Figure 1-1(b).

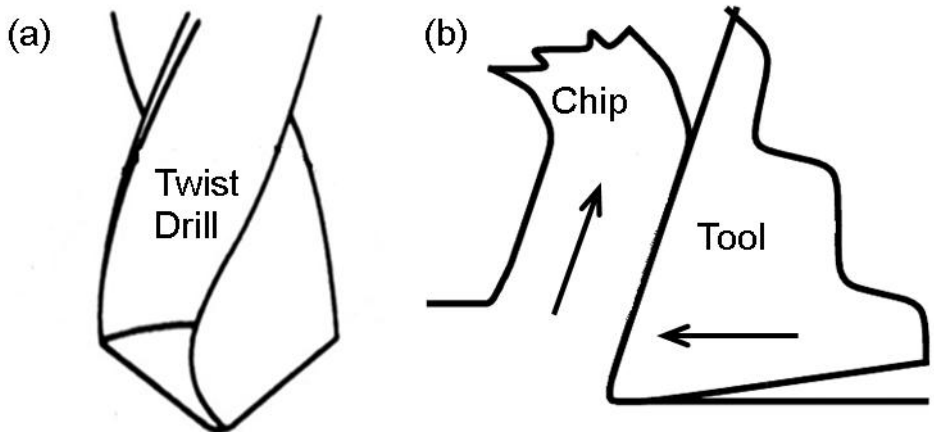

Figure 1-1. HSS cutting tools (a) twist drill and (b) orthogonal cutting.

Figure 1-2 shows the manufacturing process of a HSS twist drill from material in the as-received condition and drawn to size with interstage sub-critical anneals (below the recrystallization temperature 780 ℃) between each draw to prevent breaking due to work hardening of the material. Once the nominal diameter is achieved, the material is vacuum heat treated to achieve the desired hardness. When completed, the twist drill can be surface modified to enhance its performance depending on the application and design of the twist drill.

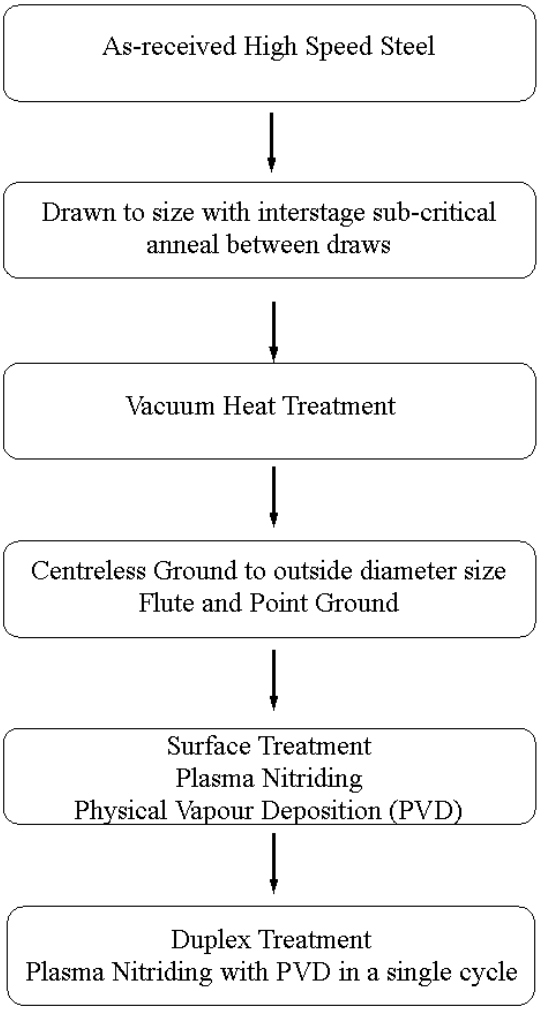

Figure 1-2. The manufacturing process from as-received HSS material to finished twist drill with post manufacturing treatments of plasma nitriding or PVD coating or combined 'duplex' treatment.

1.1.1 The history of HSS

Iron manufacturing can be traced to early refining methods such as potting and stamping and to even earlier (around 800 BC) charcoal and Bloomery processes. These were replaced by the puddling method in the 1800s which allowed an increase in iron production in Great Britain. Wrought iron from puddling was used, for example, to construct the Clifton Suspension Bridge in Bristol (1864), to provide the framework for the Statue of Liberty (1886) and to construct the Eiffel Tower (1889). Open Hearth Furnaces first developed in the 1850s were replaced by the Basic Oxygen Furnace BOF, offering faster processing and commercialized in the 1950s. These were eventually superseded by the electric arc furnace that while slower, offers better control over temperature and oxygen content,

yielding a higher quality steel [14]. When Iron is alloyed with carbon it becomes steel and steels remain the most important group of metallic alloys, possessing a wide range of microstructures and mechanical properties.

Trent [15] describes the 1760s as being the first major era in the development of metal cutting. Not surprisingly this coincides with the beginning of the industrial revolution in Britain [16]. Metal cutting was performed using high carbon tool steels that were prone to early life failure even at slow cutting speeds. Demand for increased production rates created a demand for higher tool performance and encouraged the materials research which continues to this day. In 1868, Mushet [15] found that by adding tungsten to carbon tool steel, the same hardening response was achieved in air cooling as was achieved in conventional carbon tool steel when quenched in brine or oil. In 1900, Taylor and White[17], in the United States, were heat treating to temperatures higher than was considered desirable at the time with the result that these steels retained hardness at much higher temperatures, allowing higher cutting speeds and greater depth of cut. The first High Speed Steel was so named due to its capacity to cut at higher speeds and feeds than the previous plain carbon cutting tools. Known as 18-4-1 or T1 and patented in 1910, it had a composition of 18 weight percent (wt. %) W, 4 wt. % Cr, 1 wt. % V, 0.7 wt. % carbon with the balance Fe [18]. During the Second World War, materials shortages and higher cost encouraged development and use of molybdenum in HSS. By the 1950's there was an alternative to T1, designated as M2 and consisting of 6 wt. % W, 5 wt. % Mo, 4 wt. % Cr, 2 wt. %, 0.85 wt% C and Fe balance. Variations and additions of other alloying elements created other grades and further refinement lead to the development of Powder Metal (PM) and Hot Isostatic Pressing (HIP), all aimed at increasing performance in terms of material removal rate in cutting speeds and feeds.

1.1.2 HSS Alloying Elements

Central to the performance of HSS is the hardening response achieved during the heat treatment process. Alloying elements are introduced in quantities dictated by the intended application and by their function in the heat treatment process, whether to increase the solidus temperature or inhibit the growth of nano-sized secondary hardening precipitates, enabling higher operating temperatures.

Carbon plays an important role since interstitial solutes of carbon occupy vacancies and dislocations and combine preferentially with some of the metallic alloying elements used in HSS to form carbides [19]. Increasing carbon content lowers the solidus temperature, increases the amount of retained austenite on quenching and lowers the as-quenched hardness. Chromium is considered to be predominantly in substitutional solid solution and not tied up in the primary carbides. It is usually at around 4.0 wt. % and provides hardenability, improves tool cutting performance, retards the formation of scale during hot working and is believed to promote early nucleation of precipitates [20]. Tungsten and molybdenum are interchangeable at an atomic level and both promote resistance to tempering which gives improved tool cutting performance at higher temperatures however, too much molybdenum causes incipient melting at grain boundaries near the solidus temperature. Vanadium is added to promote abrasion resistance and to produce hard and stable carbides which being only partly soluble, release little carbon into the matrix. Cobalt does not act as a carbide former [21] however it does raise the solidus temperature, allowing higher austenising temperatures to be employed. It also promotes dissolution of vanadium carbides, improving the tool hot hardness and finer dispersions of MC and M_2C precipitates [22].

1.1.3 Primary Carbides

Since carbon greatly influences the properties of heat treated HSS, it is vital to understand its solubility and the conditions for carbide formation/dissociation as a function of temperature. The solubility limit for carbon in iron at room temperature is less than 0.003 wt. % but at elevated temperatures, it increases significantly. While some carbon exists in the substrate prior to heat treatment, the majority is locked in the primary carbides [23] and released during the heat treatment process. These primary carbides have different hardness values, seen in Figure 1-3, and dissociate into solid solution at different temperatures [24]. Goldschmidt [25] observed, using a high-temperature X-ray technique, that when starting from a fully annealed state, HSS phase changes from body centred cubic (BCC) ferrite to face centred cubic (FCC) austenite at between 850 ℃ and 900℃. While some interstitial carbon exists from the ingot manufacturing process, the majority of the carbon is tied up in

the primary carbides. These predominantly exist in the substrate as MC, M_2C, M_6C, M_7C_3 $M_{23}C_6$ and dissociate at higher temperatures, releasing carbon into the substrate.

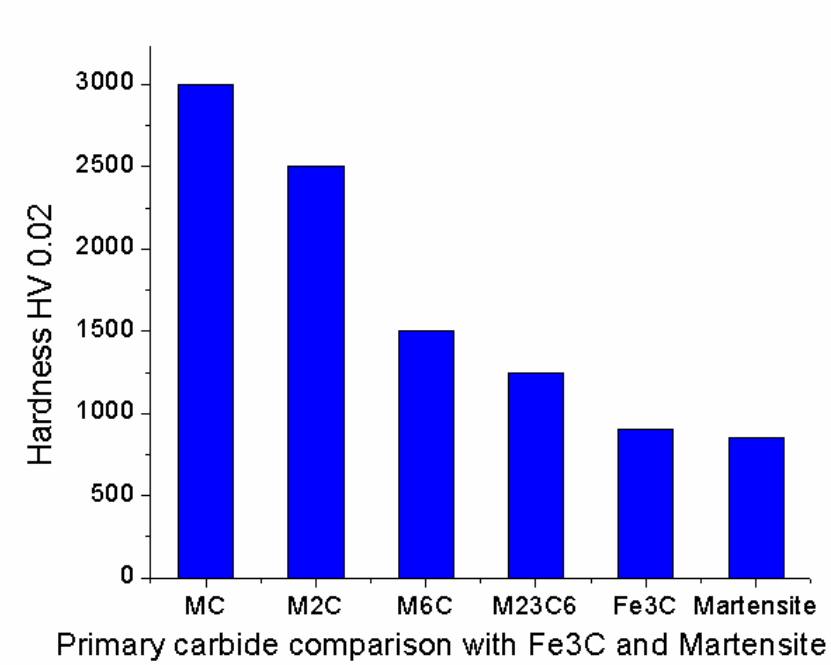

Figure 1-3. Primary Carbide Hardness [26]

$M_{23}C_6$ carbide (has a complex cubic structure where M can include Fe, Cr, Mo or W), begins to dissociate at around 900 ℃ and is considered completely in solid solution by 1100 ℃. Between 780 ℃ and 810 ℃, a transformation from $M_{23}C_6$ to M_7C_3 is known to occur [27] however, not normally formed since it requires an over stoichimetric balance of an extra 0.4 wt. % carbon [26]. M_6C where M can include Fe, W or Mo, the general range is Fe_3W_3C to Fe_4W_2C (in these formulae the W and Mo are freely interchangeable on an atomic basis). The M_6C carbide starts to dissociate at around 1150℃ and continues up to the solidus temperature. M_3C carbide is difficult to distinguish in the ferrite lattice because of its inherent small size and lattice coherency as reported by Kuo [28]. M_2C carbide (where M can include W, Mo and V) form during the ingot manufacturing process if the ingot is cooled quickly (usually avoided in normal commercial practice [29]), readily transforms to the more stable M_6C carbide. MC carbide only partly dissociates during heat treatment (where M includes V and exists as VC face centred cubic) [30] however due to stoichimetric conditions, are usually found as V_4C_3 [19] when precipitated during tempering [31].

Figure 1-4 shows an SEM image of a M35 HSS in transverse cross section, polished and nital etched. Preferential etching highlight features such as grain boundaries, primary carbides and ferritic plates or laths within the grain structure. Grain boundaries act as a barrier for the movement of dislocations during deformation loads experienced during cutting similarly to the nano-sized precipitates from heat treatment.

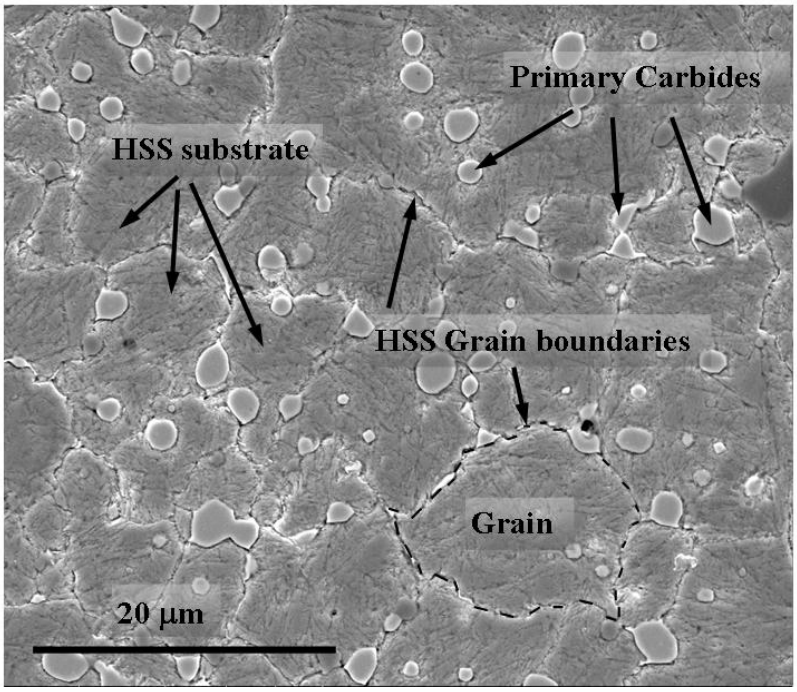

Figure 1-4. SEM image of HSS M35 substrate showing grain boundaries and primary carbides.

1.2 HSS Grades

The desired microstructure of the HSS is achieved by variation of micro-alloy wt. % and observing cooling rates from the melt to solidification [29] and the heat treatment process. Earlier grades evolved either through performance demands or material availability.

HSS manufactured as a cast ingot has a maximum size restricted to around 300 × 300 mm^2 square due to its low heat conductivity rate (e.g. 21 $Wm^{-1}K^{-1}$ for M2 HSS) [26]. The micro-structure is affected by the cooling rate from molten to solid and particular attention must be paid to cooling through the peritectic zone in order to ensure homogeneity and minimise formation of eutectics. The disadvantage

is ingot size limit, control of inclusions and carbide stringers leading to other production methods for example powder metallurgy (PM).

In this work, PM refers to a subset of standard PM processes in which the constituent powders are fabricated using water or inert gas in a molten metal atomisation method. When the melt stream is atomised by nitrogen gas, it forms small droplets with an average size of 50-100 μm which are compressed using hot isostatic pressing [32]. This method typically provides better homogeneity and can produce materials out of stoichiometric balance. Furthermore, it produces isotropic materials with almost no inclusions. The disadvantage is the cost of manufacture, hence the importance of cast ingot HSS which is a cost effective alternative.

1.3 Heat Treatment of HSS

Since the beginning of last century, the bulk of HSS heat treatment has been conducted in molten eutectic salt baths. The disadvantages of salt bath heat treatment are, through-hardening of large tool dies and the environmental impact from cleaning and disposal of waste salt.

Cold wall vacuum heat treatment (VHT) emerged in the early 1970s [33] and has been used to overcome many of the disadvantages of salt bath heat treatment. VHT has limitations for example, the need for several pre-heat stages required to reduce temperature lag throughout the entire tool during heat treatment. The holding time (typically between 150 and 180 seconds) at the austenitizing temperature, (ranging from 1160 ℃ to 1230 ℃ and dependent on the grade of HSS and the desired hardness) is critical. Time at the austenitizing temperature is required to allow dissolution of the primary carbides however too long and recrystallization (grain growth) can occur.

Hardening response of HSS in heat treatment, critical for its performance in metal cutting [34-36], is related to hardness achieved in heat treatment [26]. While Dexter [37] argues eutectic salt heat treatment gives a better hardening response, Lyapunov [38] suggests vacuum heat treatment allows better dissolution of the primary carbides at a lower temperature than salt. Leskovšek [39, 40] suggests that the tempering phase of the heat treatment plays an important role in the finale fracture

toughness of the HSS. VHT allows through-tool hardening which means the tool can be finished to a higher tolerance for high performance tools as used in CNC machining.

1.3.1 Vacuum Heat Treatment

Figure 1-5 shows a typical VHT time profile. Prior to heating, the chamber is partially evacuated using a roughing pump and backfilled with nitrogen. Heating from ambient through a number of holding temperatures to 850℃ is performed. This is the approximate limit of efficient convection heating, therefore radiant heating continues at a partial-pressure of ~13.3 Pa until the quench. An appropriate partial-pressure minimises surface oxide growth and limits evaporation of alloying elements including carbon [41-44]. VHT furnaces vary in quench pressure and gas flow type, (either circular or vertical, as shown in Figure 1-6). According to Gonçalves [45], there is an optimum pressure of 5 bar, (5×10^5 Pa) for economic quenching performance.

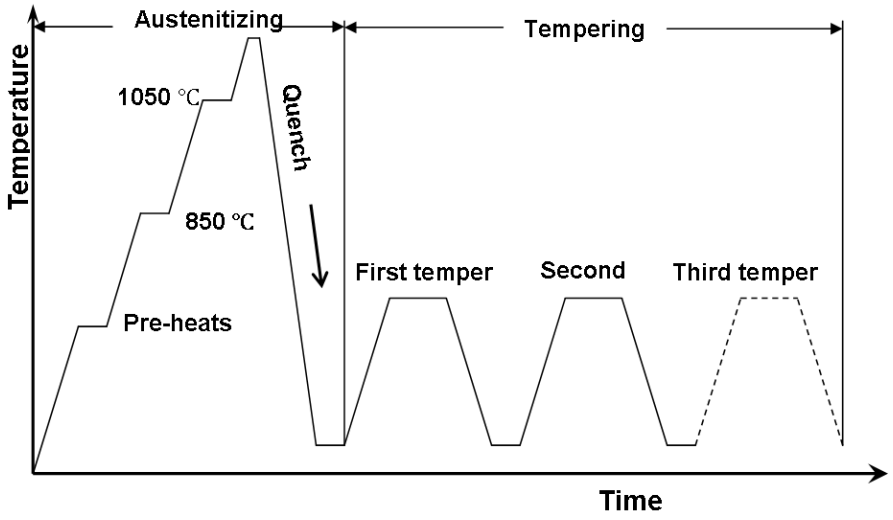

Figure 1-5. Vacuum heat treatment profile with temperature on the vertical Y axis and time on the horizontal X axis. The profile is in two parts, first is the austenitizing process and includes pre-heat holding temperatures, austenitizing temperature, quench and second is tempering where typically there are two tempers and sometimes a third temper.

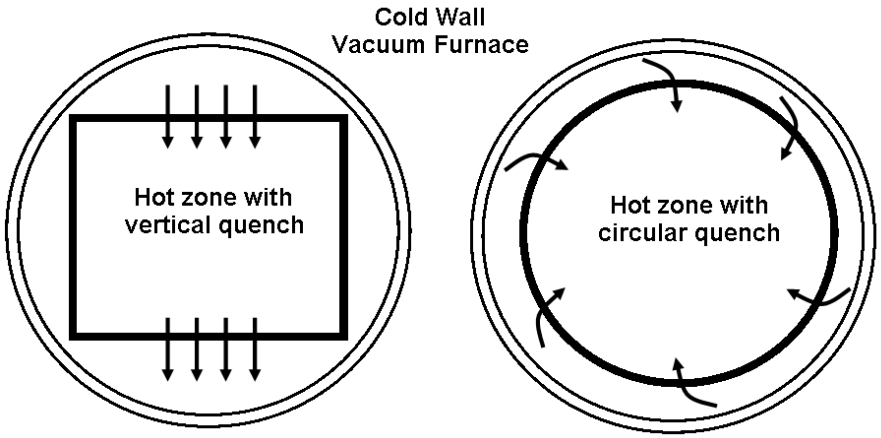

Figure 1-6. Cold wall vacuum furnace showing the hot zone with vertical and circular quench.

1.1.1.1 Hardening

Historically, smiths hardening steel (iron- carbon) 2,500 years ago were heating in a charcoal fire to 'cherry red' (820 ℃ to 870 ℃). Carbon was readily absorbed in the iron by solid state diffusion due to its small atomic size (relative to iron) and interstitial solubility. Iron (Fe) has three basic crystallographic forms; BCC (α-Fe) from room temperature to 912 ℃, FCC (γ-Fe) between 912 ℃ and 1394 ℃ and BCC (δ-Fe) from 1395 ℃ to 1538 ℃. With the addition of carbon above 0.025 wt. %, the BCC to FCC phase change occurs at 723 ℃. During the heat treatment process, the HSS substrate is ferromagnetic until the Curie Temperature (Tc) where there is a transformation to paramagnetic. The HSS ferrite Ac_1 phase change (BCC to FCC) start temperature is ~850 ℃, depending on the heating rate and composition, and the Ac_3 phase change (BCC to FCC) stop temperature is ~900 ℃, where the substrate is fully austenitic. The primary carbides, as discussed in section 1.1.3, dissociate at temperatures above ~900 ℃, releasing the alloying elements and importantly, carbon into the α-Fe substrate where it occupies interstitial positions, dislocations and vacancies. Like nitrogen, carbon has a diffusion rate several orders of magnitude larger than those of metallic alloying elements [26]. Metallic alloying elements including molybdenum, tungsten, chromium, vanadium and cobalt are nearer iron in size and therefore occupy substitional positions in the lattice. Since vanadium is in the MC primary carbide, the austenitizing temperature needs to be above ~1180 ℃ for it to dissociate.

Quenching from the austenitizing temperature back to room temperature forms meta-stable body centred tetragonal (BCT) hard but brittle martensite. The ability to form martensite is referred to as its hardenability and is dependent on material composition. A slow quench rate will form softer bainitic and pearlitic structures at the expense of martensite. This can be seen in the time temperature transformation (TTT) [14] diagram Figure 1-7 where slow cooling goes through the 'nose' of the 'C' curve. Not all the austenite transforms to martensite in quenching, so there is some retained austenite (RA).

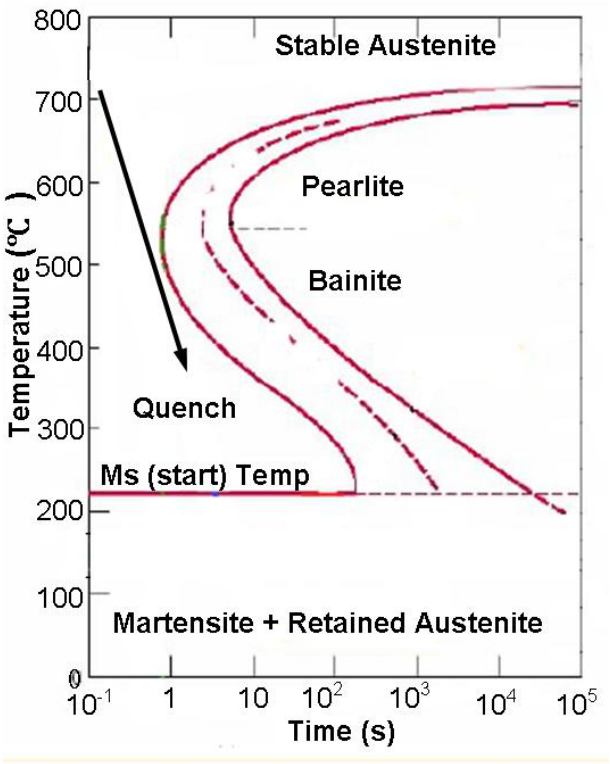

Figure 1-7. Time temperature transformation (TTT) diagram showing the quench line missing the nose of the 'C' curve, avoiding undesirable bainitic and/or pearlitic structures to form. Martensite starts to form at the Ms (start) line and cools to ambient temperature and has some retained austenite, hence the need for tempering.

Rong and Dunlop [46] using STEM/EDX analysis identified the microstructure after quenching consisting of globular primary carbides MC and M_6C up to 10 μm in diameter dispersed in heavily twinned plate martensite. The martensite plates were often separated by retained austenite with well defined orientation relations between the retained austenite and the martensite matrix. Leitner [47]

and Versaci [48] using electron diffraction identified that some M_3C carbides do precipitate at the prior austenite grain boundaries. Similarly, Rong and Dunlop [46] observed fine precipitation of cementite within the plate martensite at the internal twin boundaries concluding, the martensite auto-tempers during cooling to room temperatures.

1.1.1.2 Tempering

Tempering is a low temperature heat treatment intended to improve the mechanical properties of the material by reducing brittleness and improving toughness. There are two mechanisms in operation during tempering. Firstly, tempering of the as-quenched hard but brittle BCT martensite (also known as martensite decomposition (Figure 1-8 (a)) and tempering of retained austenite (RA) from the quench. Tempering destabilizes RA allowing it to transform to metastable martensite [49]. This newly transformed martensite requires tempering hence the need for a second or third temper. Secondly, the precipitation of nano-sized carbides Figure 1-8 (b). The mechanism of precipitation (also referred to as secondary hardening) causes needle-like, nano-sized precipitates to occupy dislocation and vacancy positions as reported by Rong and Dunlop [22, 46]. Nucleation of these precipitates generally occurs at the interface between the pre-existing cementite ferrite interface (where carbon is supplied by the adjacent cementite), at dislocations within the ferrite matrix and at pre-existing austenite grain boundaries [46].

Karagöz et al. [50] using atom probe field microscopy (APFIM) reported that during metal cutting, over-tempering caused the M_2C precipitates to coarsen too rapidly while MC precipitates were stable up to 600 ℃ over the tool life and within minutes above 700 °C. This defines the material hot hardness characteristic in cutting conditions. Metallic elements in HSS alloys move substitutionally but cannot move rapidly enough until the tempering temperature reaches ~500 °C therefore tempering is typically performed between ~530 °C to 560 °C.

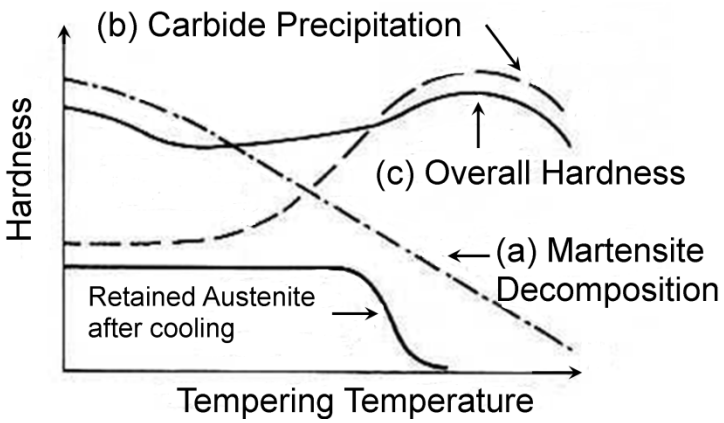

Figure 1-8. [26] Tempering curve shows the tempering and consequent decomposition of martensite (a) and precipitation hardening (b) giving an overall hardness (c).

1.3.2 Surface Oxide

Surface oxide has a mild corrosion resistance and is therefore considered useful by suppliers needing to transport and/or store their steels in ambient conditions. Surface oxide also has some beneficial tribological properties dependent on application, for example, in hot rolling [51] as a solid lubricant or in cold drawing.

Oxide is formed on the steel surface during the hot working manufacturing process and in an atmosphere that contains oxygen at elevated temperature [52-54].The surface oxide composition and thickness will depend on the workpiece temperature, cooling rate and oxygen availability [55]. The surface oxide grown below 520 ℃ generally consists of thin haematite (Fe_2O_3) on the outer surface and magnetite (Fe_3O_4) on the inner surface. At higher temperatures (up to 740℃), wustite (FeO) will form at the inner surface. Molinari et al. [56] reported that oxide growth depends on carbide volume fraction and chromium content, that is, the higher the carbide volume fraction the thicker the scale. Surface oxide growth was observed around M_2C and MC carbides and reduced around the chromium carbide M_7C [56].

Since iron (Fe) is more abundant than carbon in the substrate, during hot working, iron and oxygen combine to form FeO while at the same time the FeO reacts with the substrate carbon to form Fe and CO. This process continues as long as oxide and carbon are available. The interface between the surface oxide and substrate interface eventually becomes depleted of carbon. This ‘decarburization’ is

usually limited to the sub-surface depending on process times and temperatures [51] Figure 1-9. If the oxide has low permeability, the carbon can be prevented from diffusing out of the substrate [57] but this is rarely observed during commercial processing.

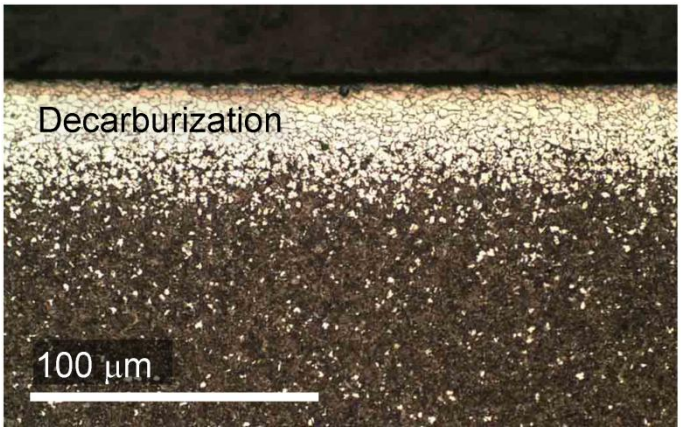

Figure 1-9. Optical image of cutting tool steel, cross sectioned, polished and etched. The top of the image is the surface and moving down, the decarburization zone can be observed as white.

Stout and Aho [58] observed that decreasing the oxygen potential could give rise to greater decarburisation depth (Figure 1-9) and Leprince et al. [59] found that carbon dioxide could form by interacting with the surface oxide and/or atmospheric oxygen to form carbon monoxide. Carbon is therefore described as a reducing agent for iron oxides [60-62]. According to the Ellingham diagram of Gibbs free energy (a measure of the thermodynamic driving force that makes a reaction occur), the production of CO_2 reduces as it becomes more stable. Above 720 °C, CO is more likely to occur [63] due to the Boudouard reaction [64] (Figure 1-10).

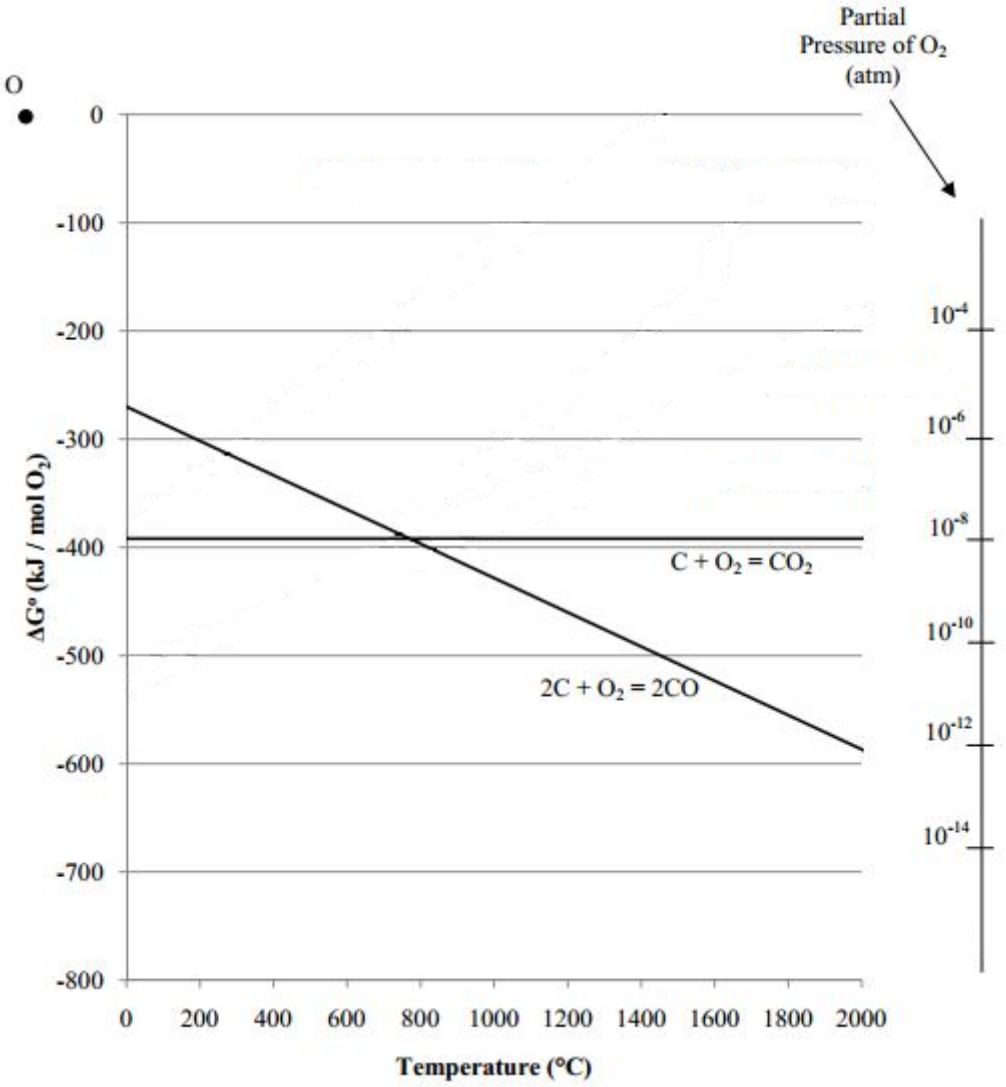

Figure 1-10. Ellingham diagram [65]

Previous work [52, 60, 61] shows reduction can occur at lower than 765 ℃ however, since the carbon in HSS is primarily contained in the M_6C primary carbides [6, 29] it cannot contribute to oxide scale reduction at temperatures below that for primary carbide dissolution.

Previous investigations of loss of carbon in HSS are limited to hot working in an oxygen environment and annealing. This part of the thesis investigates the primary cause of poor hardening response of M35 HSS in VHT which in turn affects cutting performance.

1.4 Nitriding

To further improve HSS cutting performance, surface engineering using salt bath and gas nitriding have been available since the middle of last century [66] with the first nitriding patent applied for in 1908 [67]. Essentially, they involve the dissociation of ammonia NH_3 when in contact with a heated alloyed steel workpiece. The hot substrate acts as a catalyst causing molecule dissociation and the active nitrogen introduced at the surface diffuses to interstitial positions in the iron, eventually forming fine precipitates of alloy nitrides. Nitridable steels contain elements including chromium, aluminium, molybdenum, vanadium, and tungsten since these easily form nitrides [67]. The region in which precipitation occurs is called the diffusion zone. Typical nitriding produces a 'bright' finish above the diffusion zone. At higher nitrogen concentrations, a 'compound layer' forms at the surface (see Figure 1-11), sometimes referred to as the 'white layer', that can be engineered to generate improved tribological properties [68]. Extending the nitriding time or increasing the nitriding potential will result in a more pronounced compound layer. The latter contains a mixture of γ' (gamma prime) and ε (epsilon) or primarily ε. The benefits of nitriding include improved tool life, high fatigue strength and improved corrosion resistance [69].

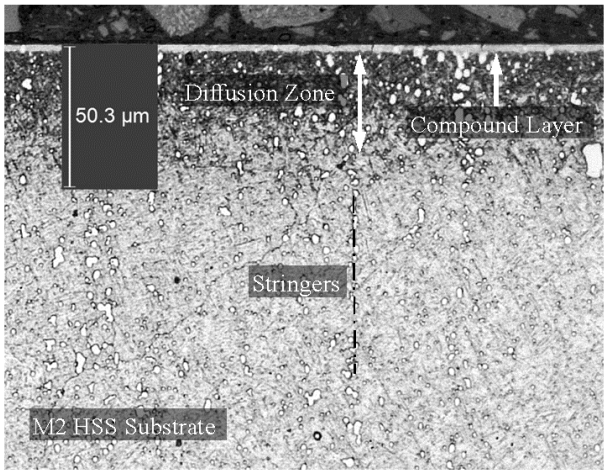

Figure 1-11. Nitrided M2 HSS coupon in longitudinal cross-section, polished and etched to reveal the compound layer and diffusion zone. Also observable are primary carbide stringers.

The FeN_x (Nitrogen Iron) phase diagram is shown in Figure 1-12. The FCC phase, although having a higher atomic packing factor compared with the BCC phase, has two interstitial sites; the octahedral

and tetrahedral sites with radii of 0.28 Å and 0.52 Å, respectively [70]. Cahn [70] suggests nitrogen occupies the smaller octahedral site since there are fewer neighbouring iron atoms to interact with. The solubility limit of nitrogen in iron is temperature dependent and the initial phase of Fe_4N - γ' is precipitated up to 0.1 wt. % N and below 585 ℃. Above this concentration and between 5.7 and 5.9 wt. % N, Fe_4N - γ' forms as a single-phase field. Increasing the N concentration past 5.9 wt. % results in the precipitation of epsilon ($Fe_{2-3}N$ - ε) and around ~7.6 wt. % N, the iron nitride exists as a single phase. This is strongly influenced by the carbon content of the steel; increased carbon makes the ε phase more probable. The equilibrium diagram shows that control of the nitrogen diffusion is critical to process quality [67]. Advances in nitriding technology have given advent to gas, salt bath nitriding, Nitro-Carburising [71] and plasma nitriding including Active Screen Plasma Nitriding (ASPN) patented by Georges in 1999 [72]. These processes are all aimed at achieving a hard but tough diffusion zone to enhance the tribological characteristics.

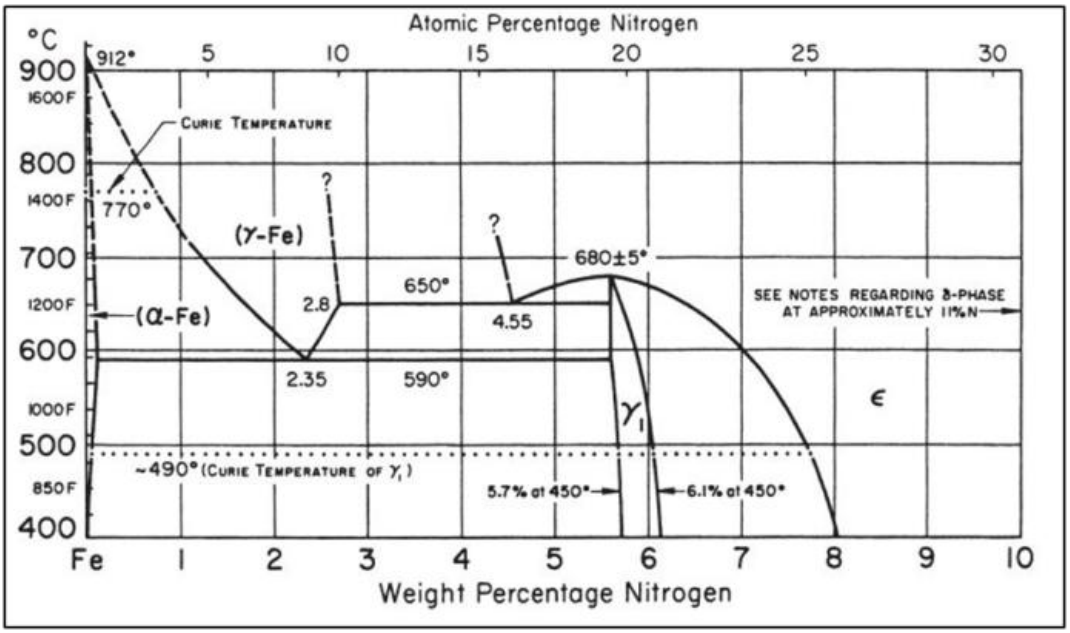

Figure 1-12. Phase Diagram of Nitrogen solubility in iron [67]

1.4.1 Plasma Nitriding

Plasma Nitriding was patented by German physicist, Berghaus [73, 74], who developed the "glow discharge" method in 1932 [73]. Plasma nitriding has gained significant market share since the late 1960s with the introduction of DC glow discharge nitriding [75] enabling improved hardening

response and reduced processing times. Advances in power supply and control technologies further assisted the process in gaining industrial acceptance [67]. The hardening response achieved during plasma nitriding depends on temperature but also on other factors [76-78]. Muratore [79] investigated the ionization states present in electron beam generated nitriding plasmas (at 10mm from the plasma source) and observed predominantly N_2^+, secondly N^+ and to a lesser extent Ar^+. For <1000 eV, ion bombardment is linearly proportional to the magnitude of the N_2^+ ion flux. The average energy of the ions incident on the surface is dependent on their mean-free path which is determined by the chamber pressure [80]. Hence, the hardness achieved after plasma nitriding can decrease at higher process pressures [81].

HSS is a particularly challenging steel to nitride since it contains several different nitridable alloying elements. Nitriding at a high potential or for too long, can result in early tool life failure due to edge effects, hollow cathode effects and/or decarburisation in the diffusion zone. Problems with DC glow discharge relating to hollow cathode discharges limited the development of the technique [82, 83]. In active screen plasma nitriding systems [84], the ionizing potential was applied to a screen hence reducing the need for a high potential on the work piece. However, scaling the method to industrial scale is problematic [83, 84] and sputtering of the screen itself is followed by deposition of this material onto the workpiece(s) [85]. Edge effects are caused by electric field enhancement at edges leading to increased local current density and higher temperature. The higher nitriding potential promotes a deep and brittle diffusion zone, resulting in increased hardness at the expense of toughness [86]. In addition, partial decarburisation in the diffusion zone can lead to the formation of Fe_3C networks at the diffusion zone boundaries [87]. Plasma nitriding is typically performed at voltage-biases of up to -500 Volts [86, 88-92], between 20 Pa to 500 Pa [69, 87, 93-95] and times of between 2 and 20 hours [78, 96, 97].

1.5 Duplex Coatings

The first commercial Physical Vapour Deposition (PVD) coatings were used in the metal cutting industry in the early 1980s, although it would take another 10 years for more widespread acceptance

[98]. Unlike Chemical Vapour Deposition (CVD), developed in the 1950s, which required coating temperatures of 1000 ℃ to 1100 ℃, PVD could be performed at around 500 ℃, making it suitable for HSS. Bunshah [99] patented the Activated Reactive Evaporation (ARE) process which was further developed to include a tool voltage-bias, emphasising the importance of ion-deposition in the PVD process. Two principle deposition techniques were used to generate the vapour phase, categorised as evaporation and sputtering. Methods of evaporation include direct resistance heating, electron beam, laser beam, radiation, eddy current and cathodic arc evaporation with electron beam evaporation and cathodic arc discharge evaporation being the more commonly employed techniques used in tool manufacturing. Electron beam evaporation can be achieved by either hot-filament thermionic electron beam or by a plasma sourced electron beam (using either a cold cathode plasma electron beam or a hot hollow cathode discharge beam). Cathodic arc evaporation (CAE), described in detail by Anders [100], can be from a pulsed or continuous (random or steered) arc source. Macro-particles are generated in CAE [101, 102] and are included in the deposited coatings. However, the high degree of ionisation of the plasma [103] promotes adhesion to the substrate through higher energy transfer [104].

The first ceramic PVD coating employed for tool applications was TiN [105-107]. Higher cutting tool feeds and speeds were offered over HSS due to the higher hardness ~2500 HV and improved tribological properties of TiN. Further development of PVD led to high performance TiAlN [108], CrN [109], AlCrN [110] and TiCN [111] tool coatings. Adhesion [112], thermal stability [113], lattice mismatch [88, 114] and high internal stress [115] all contribute in imposing a coating thicknesses limit of 2-4 μm [116]. Above this, delamination and reduced tool life is likely. Research in PVD for tool applications has increasingly focussed on functionally graded coatings [117], in which the lattice mismatch caused by attaching a hard ceramic coating to a relatively softer substrate is alleviated. Subsequently, metallic interlayers [118] have been added to improve adhesion and toughness with only slightly reduced hardness [119] while interrupted coatings [120] attempt to reduce internal stresses for increased coating thickness.

Duplex coatings (see Figure 1-13) consisting of a nitrided HSS substrate and a hard refectory PVD coating, can exhibit the high hardness and high wear properties of PVD coatings combined with the

enhanced fatigue resistance and load carrying properties of the nitrided substrate [92, 121]. They have provided improvements in tool cutting performance largely due to enhanced substrate support of the PVD coating [122] (Chapter 4). Opinion is divided on the role of the compound (white) layer resulting from nitriding and its effect on the adhesion of the PVD coating. Podgornik et al. [123] reported that a uniform, dense and well adhered compound layer was beneficial in their duplex coatings while Yang et al. [124] produced a functionally graded CrAlN PVD coating using an Active Screen Plasma Nitrided (ASPN) stainless steel substrate without a compound layer and achieved similar performance improvements. In early duplex research, plasma nitriding was conducted in a separate process chamber to PVD coating [86, 91, 92, 125]. Contamination between processes was inevitable, leading to reduced adhesion of the PVD coating. Sato et al. [126] modified a single chamber to perform duplex coating with good results however they opted to avoid hydrogen etching which is described by Figueroa [76] as etch cleaning the surface, hence promoting the nitriding process and improving adhesion**.** Figure 1-13 shows a SEM image of a HSS coupon in transverse cross section. A duplex treatment of plasma nitriding with a PVD coating can be observed. From the top of the image down, a 2-3μm TiAlN PVD top coating can be observed and connected to a 0.5 μm TiN interlayer. Below the TiN interlayer the diffusion zone can be seen to extend into the HSS substrate.

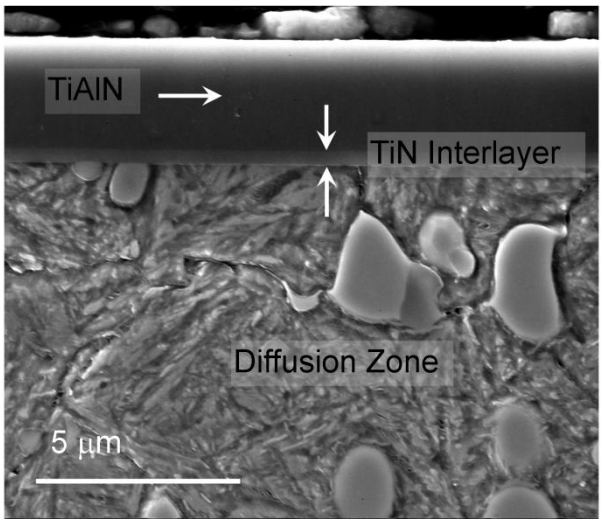

Figure 1-13. Duplex coating showing 2-3μm TiAlN PVD coating with 0.5 μm TiN interlayer above the HSS plasma nitrided diffusion zone.

While duplex coatings have been investigated previously, there is limited research on in-situ duplex coatings in an uninterrupted single cycle. This part of the thesis explores performance of an in-situ duplex treatment of M2 cutting tools using a low pressure, low voltage-bias to address edge effect and ensure a nitrided diffusion zone gives support for the PVD coating which is previously reported as undergoing plastic deformation under cutting conditions leading to PVD coating delamination and lower cutting performance.

1.6 Thesis Aims and Objectives

The thesis describes an investigation into improving HSS cutting tool performance. The first objective was to investigate the structural and chemical changes occurring during industrial-scale vacuum heat treatment of HSS. The response of HSS to heat treatment has been reported [19, 26] however, the hardening response of HSS in VHT requires a material in which the balance of the alloying elemental content is within tolerances specified by the supplier. Material characterisation was by a combination of techniques including combustion infrared absorption spectroscopy [127], Scanning Electron Microscopy (SEM), and mechanical analysis by Vickers Hardness HV30, micro-Vickers HV0.1 hardness testing. Performance characterisation was made using accelerated drill testing. Further investigation focused on the presence of surface oxide and its effect on hardening response in VHT. Material characterisation was by SEM, X-ray diffraction (XRD), Hardness Rockwell C (HRC), Differential Scanning Calorimetry (DSC) coupled to Thermogravimetry Analysis (TGA) and Evolved Gas Analysis (EGA) and mechanical analysis by micro-hardness.

The second main objective of this work was to investigate improvement in cutting performance of HSS using a duplex treatment of PVD coatings on a nitrided HSS substrate using a Balzers INNOVA cathodic arc evaporation PVD system. Nitriding was investigated with respect to gas ratio, pressure and voltage-bias and following this, TiAlN coatings were implemented as part of a duplex process conducted in one chamber as a single process. Structural characterisation was then performed using XRD, X-ray photoelectron spectroscopy (XPS), infrared absorption spectroscopy after combustion in an induction furnace [129], electron microscopy, Verein Deutscher Ingenieure VDI [128] and atomic

force microscopy (AFM). Micro-hardness and nano-indentation measurements revealed the mechanical properties of the duplex coatings and nitrided/coated comparison samples. Accelerated drill testing was once again used to measure tool cutting performance. Standard drills, nitrided, PVD coated-only and duplex (single cycle plasma nitriding/PVD coating) drills were tested.

The main aims of the investigations in this thesis are as follows:

- Investigate the mechanisms leading to variable hardening response of HSS in VHT.

- Implement plasma nitriding in an INNOVA PVD coating chamber using novel low pressure, low voltage-bias and determine the nitriding response with respect to up-stream flow control versus down-stream throttle control. Determine the nitriding response with respect to pressure and the effect of voltage-bias.

- Elucidate the performance benefits offered by duplex treatments.

1.7 Thesis outcomes

The major outcomes of this work include:

- Advanced understanding of HSS response to VHT with respect to carbon content (at. wt. %)
- Advanced understanding of central plasma nitriding and HSS response in nitriding using low pressure low voltage-bias.
- Advanced understanding of the effect of the interaction between a nitrided HSS substrate and an inter-layered PVD coating shown in improved performance in accelerated drill testing.

1.8 Thesis outline

Chapter 2. “Vacuum Heat Treatment of High Speed Steel Cutting Tools” [129]. This chapter details an investigation into poor hardening response of HSS in VHT. The work examines issues of carbon loss and attributes this to high strain deformation in cold drawing in combination with the presence of a surface oxide that exists on the material ‘as received’ from the supplier. Accelerated drill testing is used to characterise the hardening responses and corresponding differences in performance.

Chapter 3. “Carbon Evolution during Vacuum Heat Treatment of High Speed Steel” [130]. This paper describes an investigation into the evolution of CO during VHT and its correlation with thickness of surface oxide layer present during VHT and ultimately, with hardness after VHT.

Chapter 4. “Microstructural and tribological characterisation of a nitriding/TiAlN PVD coating duplex treatment applied to M2 High Speed Steel tools” [122]. In this paper, duplex coating of TiAlN on a plasma nitrided HSS substrate is described. Accelerated drill testing reveals the cutting performance of the duplex treatment with comparison to coated-only, nitrided and standard drills. Microstructural measurements are used to support this comparison.

The thesis concludes by summarising the results highlighted in the three preceding chapters and link these results as a whole to the central idea of improved performance of HSS cutting tools. Areas for future work are also suggested.

Chapter 2. Vacuum Heat Treatment of High Speed Steel Cutting Tools [129]

Vacuum heat treatment of high speed steel cutting tools

A. Rousseau*, E. Doyle and D. McCulloch

An investigation of under hardening of small diameter HSS drills following vacuum heat treatment is presented. Poor hardening response was found to correlate with a loss of carbon in the HSS blanks. It is shown that full hardness could be attained by removing up to 200 μm off diameter prior to vacuum heat treatment. Metallographic examination revealed that the probable cause of carbon loss was the presence of oxide scale which set up a diffusion gradient leading to rapid grain boundary diffusion of carbon. Accelerated drill testing revealed that the under hard drill had a low tool life but with lower variance. The fully hardened drills exhibited higher variance largely due to the occurrence of early life failures. Metallographic examination suggests that the latter is due to the presence of large defects in the form of fractured primary carbides formed in the drawing process.

Keywords: Hardening response, Vacuum heat treatment, High speed steel, Carbon depletion, Drill testing

This paper is part of a special issue on 'Developing the world of tooling'

Introduction

High speed steel (HSS) is a complex alloy tool steel accounting for over 30% of the global cutting tool market. Critical to the performance of HSS cutting tools is the heat treatment cycle, that is, preheat, high heat, quenching and multiple tempering. Throughout the last century the bulk of HSS heat treatment was conducted in salt baths. The latter is ideally suited to in-line or carousel heat treatment of HSS. Fixtures can be designed such that only the fluted section of the cutting tools are hardened and tempered while the shank remains relatively soft. Such fixtures have the added advantage of easy exploitation of gravity to reduce distortion while tools are held at high heat. Disadvantages of salt bath heat treatment relate to issues of waste, the need for washing of heat treated tools and difficulties when there is a need for through hardening over the whole tool. To overcome these disadvantages vacuum heat treatment was increasingly used towards the end of the last century. It does however have its own limitations; in particular, distortion is of major concern. Also, fine details concerning the heat treatment cycle become more problematic, for example, the need for several preheats on the way up to the hardening temperature and the appropriate holding times especially at high heat. The quench rate is not well defined by steel suppliers who recommend only generalised guidelines for the heat treatment of the many grades of HSS in vacuum heat treatment (VHT). This is not surprising given the wide variations in high pressure gas quenching capacity in modern vacuum heat treatment furnaces and hence the quench rate needed to achieve full hardening response in HSS.[1]

Clearly a major concern in the heat treatment of HSS cutting tools is the hardening response. In this regard it would appear that salt heat treatment would be the preferred option given the more efficient heat transfer, the shorter holding times at high heat and a more efficient quench. However Lyapunov[2] suggested that in VHT the inevitably longer holding times between the preheats and the final high heat allows for lower hardening temperatures leading to more dissolution of primary carbides which, in turn, should yield a better hardening response. It was within this context that the authors experienced difficulties in attaining appropriate hardening response in the manufacture of small diameter drills when the heat treatment route was changed from salt to VHT. This paper details an investigation of the changes in hardness with changes in the processing method along with the metallographic and chemical analysis conducted in an attempt to determine the cause of under hardening. Accelerated drill testing was carried out as a means of assessing the performance of drills manufactured under different conditions.

Experimental

The investigation was conducted on M35 HSS drill blanks used in the manufacture of small diameter drills, that is, drills less than 5·0 mm in diameter. Bulk composition of alloying elements in the M35 material was checked by the LECO combustion method[3] in the as received condition before VHT. See in Table 1 below.

Drawing process

HSS M35 coil, approximately 5·0 mm in diameter, was received from the steel supplier and drawn up to four times on a pull block machine with a lead-in draw die

Applied Science (Physics), RMIT University, Melbourne, Australia

*Corresponding author, email arousseau@sutton.com.au

Published by Maney on behalf of the Partnership
DOI 10.1179/1749514813Z.00000000070

Table 1 Composition of as received M35 HSS coil before VHT

Material/wt-%	Fe	C	Si	Mn	Cr	Mo	V	W	Co
M35 as received	Balance	0·91	0·61	0·28	4·7	4·56	1·63	5·8	4·12

Table 2 Diameters of drawn HSS material showing percentage reduction in area for each draw

Diameter/mm	Area mm^2	% reduction in area
5·0	19·63	…
4·6	16·62	15·36
4·25	14·19	14·64
3·78	11·28	20·48
3·48	9·79	13·25

angle of 18 degrees. The reductions in diameter and in cross sectional areas for each draw is shown in Table 2 below. The lubricant used in the drawing process was soap. Following each draw pass the material was annealed at 780°C in a nitrogen gas recirculating furnace.

After the final draw and anneal, the HSS was straightened and cropped to lengths of 3·6 m. These lengths were then machined on a CNC lathe to generate blank lengths of 40 mm.

Vacuum heat treatment process

HSS samples from each draw size were then heat treated using a commercial Abar Ipsen Vacuum heat treatment furnace with a capacity for high pressure gas quenching up to 6 bar. The samples were packed in stainless steel rolled hollow square section measuring $50 \times 50 \times 65$ mm long, as per standard commercial operation. The VHT cycle used is summarised in Table 3.

Carbon loss analysis

Given the concerns about hardening response of the HSS, it was considered essential that some measure be made of the carbon content after annealing and after vacuum heat treatment. M35 drill blank samples were taken from each draw size and analysed for carbon content, using the LECO combustion chamber method, with each reading being the average of five measurements. It should be noted that this method essentially measures the bulk carbon content.

Table 3 Vacuum heat treatment cycles for M35 material

M35 VHT cycle	Temp/°C	Hold time/min	Pressure/bar
Preheat	550	120	2
	850	90	2
	1050	50	10×10^{-4}
High heat	1190	3	10×10^{-4}
Quenched	40	30	5
Temper	550 × 3	180	2

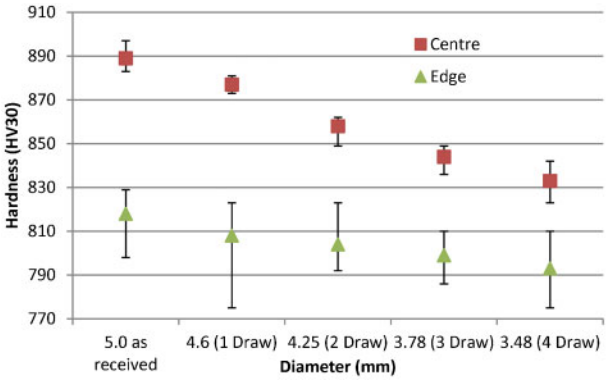

1 Graph of hardness as function of drawn diameters and number of draws showing trend of falling hardness at centre of HSS blanks along with low hardening response at outer diameter

Metallographic analysis

Metallographic analysis was conducted on selected HSS blanks before and after vacuum heat treatment. The blanks were cross-sectioned with an abrasive cut-off wheel using high flow coolant. Samples were mounted in a phenolic resin and polished using diamond abrasive laps, finishing with 0–1 μm diamond on a napped cloth. Where appropriate, samples were etched in 4% nital. Microstructural analysis was conducted using both optical and scanning electron microscopy (SEM). Hardness (HV30) measurements were conducted on the polished cross-sections. Each hardness reading is an average of five measurements.

Accelerated drill testing

Accelerated drill testing was carried out on two groups of M35 HSS drills measuring 2·9 mm in diameter, as a means of providing some guide to performance as a function of different manufacturing conditions. The first group (group 1) was produced from 3·48 mm diameter 4 draw M35 HSS blanks. The second group (group 2) was produced from 3·78 mm diameter 3 draw M35 HSS blanks machined to a diameter of 3·48 mm. The vacuum heat treated blanks from groups 1 and 2 were flute and point ground as one batch on the same CNC grinding machine. Accelerated drill testing was done on a quenched and tempered cold work tool steel plate (specification P20 supplied with a nominal hardness of 300 HV30). The test conditions are shown in Table 4. The accelerated drill tests were conducted on a CNC machining centre. The test machine was programmed to randomise the location of the holes over the drill plate.

Table 4 Accelerated drill test conditions

Material	Cutting speed V_c/m min^{-1}	Feed/mm rev^{-1}	Hole depth
P20	35	0·14	2·5D (7·25 mm)

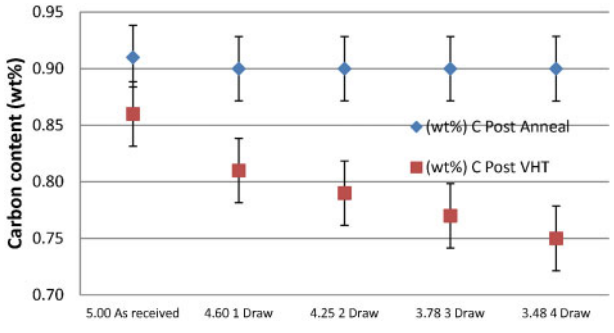

2 Graph of carbon content as function of drawn diameters and number of draws for HSS blanks after annealing and after VHT showing that carbon loss occurs after VHT and not after annealing stage

Results and discussion

The hardening response for the HSS blanks as a function of the number of draws after VHT is shown in Fig. 1. The latter shows a difference in hardening response from the centre of the HSS blank to the outside. In addition hardness at the centre of the blanks shows a consistent fall with each increase in the number of draws, a trend not so clearly shown by the outer diameter, possibly due to the greater scatter in the results. It is evident, however, that it is the material in the outer diameter of the drill blanks that shows poor hardening response, that is, hardness values in the range of 770–800 HV30.

HSS blanks were selected from each of the four draws and analysed for carbon. It should be recalled that the latter technique gave a measure of the bulk carbon content. Two sets of samples were analysed, the first after the interstage anneal (that is before VHT) and the second set, after VHT. The results are shown in Fig. 2. It is evident that there is a trend of reducing carbon content with increase in the number of draws. There is little or no change in the carbon content with each draw and interstage anneal. This makes clear the fact that the loss of carbon is not occurring as a result of poor atmosphere control during the interstage anneal.

As is evident from the above results the poor hardening response observed at the outer diameter of the HSS drill blanks correlates with a fall in the carbon content. With a view to examining this correlation further, HSS blanks measuring 3·48 mm in diameter

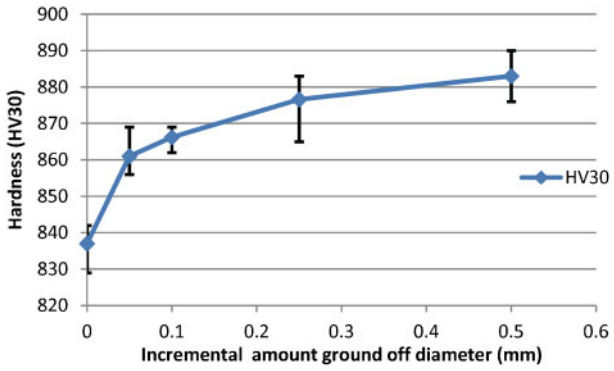

3 Graph of hardness against material removed from outer diameter of 3·48 mm diameter drawn HSS blanks showing consistent rise in hardness with amount of material removed

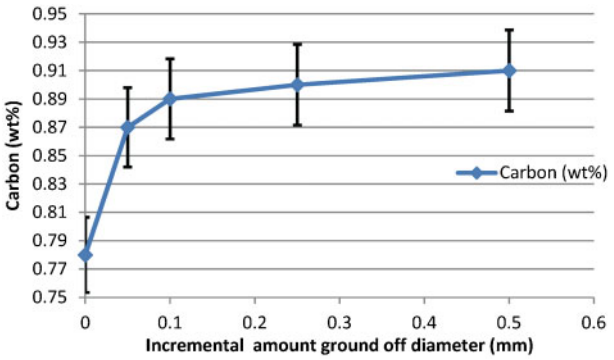

4 Graph of carbon content as function of amount of HSS removed from outer diameter of HSS blanks showing significant rise in carbon over first 50 μm and slower rise thereafter

(that is taken after 4 draws and 4 interstage anneals) were centreless ground to produce four sets of HSS blanks in which the first set had 50 μm removed from the outer diameter, the second 100 μm, the third 250 μm and the fourth 500 μm. These blanks were then hardened and tempered in VHT as previously. The hardness results are shown in Fig. 3. There is a rise in hardness with increase in the amount of material removed in grinding.

HSS blanks were taken from the above four sets and analysed for carbon content. The results are shown in Fig. 4. There is a significant rise in the carbon content after removal of the first 50 μm from diameter followed by a smaller rise up to the limit of the test, that is, removal of 500 μm of HSS from the diameter.

Figures 3 and 4 are important findings since they establish that for the HSS investigated in this study the removal of up to 100 μm for the outer diameter resulted in the retention of higher levels of carbon after VHT. Once such carbon levels are re-established to the levels present in the as supplied coils then a good hardening response is achieved following VHT.

In seeking explanations for the poor hardening response and the loss of carbon after VHT several of the HSS blanks were examined metallographically.

Figure 5 shows the microstructure of polished and etched cross-sections of HSS blanks after VHT in the as received condition (Fig. 5*a*) and after four draws and interstage anneals (Fig. 5*b*). It is evident from Fig. 5*a* that the HSS blank has an oxide scale at the surface approximately 20 μm in thickness. It should be noted that the oxide scale was present on the coil in the as received condition from the steel supplier. The oxide scale is also present on the HSS blank after four draws and interstage anneals as shown in Fig. 5*b*. In the latter, the condition of the scale is however much deteriorated in the form of open grain boundary structure and porosity. Another point of difference is that the oxide scale after the drawing and annealing has a series of large lateral cracks running at right angles to the length of the blank, see Fig. 6*a*. These cracks appear to be contained within the thickness of the oxide scale, as shown in Fig. 6*b*.

According to Hoyle[4] the presence of oxide scale on the surface of HSS can lead to rapid decarburisation during heat treatment. Such an explanation would account for the results obtained in the present investigation. Indeed,

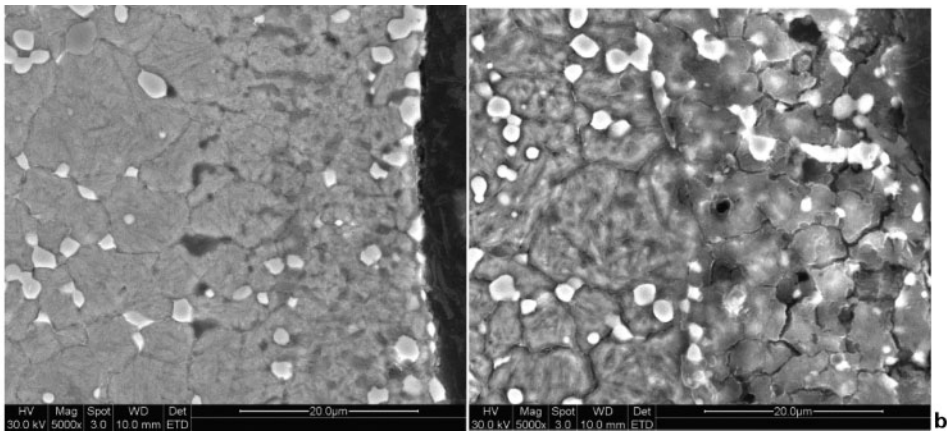

a 5·0 mm diameter M35 as received post-VHT; *b* 3·48 mm diameter M35 4 draw and anneal post-VHT

5 Images (SEM) of polished and etched cross-section showing presence of 20 μm scale

closer examination of the boundary region between the oxide and the HSS substrate in Fig. 5*b* shows, not surprisingly, that the grain boundaries in the scale and the HSS substrate are contiguous. This provides a chemical diffusion gradient for rapid grain boundary diffusion of carbon which explains the porosity present in the scale. Add to this the fact that the loss of carbon increases with increasing reduction in diameter of the blanks after drawing can be simply accounted for on the fact that the scale plays an increasingly greater role as the surface to volume ratio increases with each reduction in diameter.

The fact that the loss of carbon was more evident after VHT than after salt heat treatment appeared at first sight in the investigation to add fuel to the continuing debate on the benefits and disadvantages of vacuum versus salt heat treatment.[1,5] In fact, the explanation is self evident in the light of the present findings. In salt heat treatment, the immersion time in the high heat of 1190°C, after the first preheat at 850°C, is of the order of 100 s. Whereas, in vacuum heat treatment, the elapsed time in the furnace between the last preheat of 1050°C and the high heat of 1190°C is of the order of 1·5 h. Diffusion is critically influenced by time at temperature and hence the greater loss of carbon after VHT.

The major finding of this investigation in the production of small diameter drills is that oxide scale present on the as received HSS coil material provided a chemical diffusion gradient driving the loss of carbon and hence a poor hardening response following VHT. Support of this finding can be found in Fig. 4 above in which it is evident that the removal of 50 μm from the diameter (that is 25 μm off the surface) results in a significant improvement in carbon retention. Interestingly the carbon retention continues to improve with further removal of HSS substrate material. It is a matter of speculation but this could be related to the defect structures generated in the outer surface layers during drawing. A similar finding was reported by Yanagisawa *et al.*[6] in their study on the effect of drawing on the hardness response of HSS wire. However, in the study they did not measure the carbon content and concluded that the lack of hardening response was due to voids generated by fractured carbides over 5 μm in diameter (on average) in the microstructure.

As indicated in the section on 'Introduction', accelerated drill tests were conducted with a view to determining differences in performance of the drills as a function of the method of manufacture. Two groups of M35 HSS drills measuring 2·9 mm in diameter were manufactured such that group 1 was essentially under hard, that is less than 800 HV30. While group 2 were fully hard, that is, above 850 HV30. The accelerated drill test results are shown in Fig. 7. The drills in group 1 show a relatively low tool life in terms of the number holes to failure and lower variance. The results for drills in group 2 are very different. Some drills showed a very large tool life while several failed early. It is possible that the early life

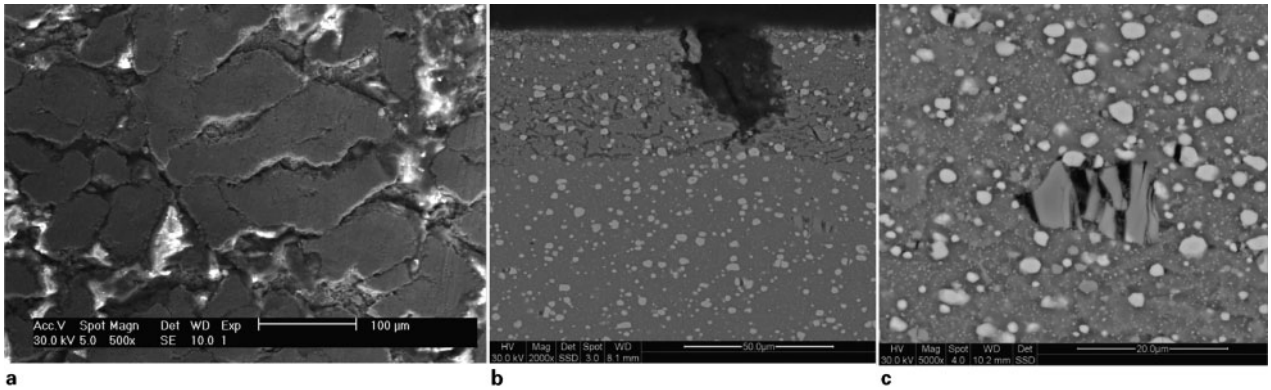

a 3·48 mm diameter surface using back scatter; *b* 3·48 mm diameter longitudinal mounted showing scale cracking; *c* 3·48 mm diameter longitudinal mounted showing fractured primary carbide

6 Images (SEM) of surface scale

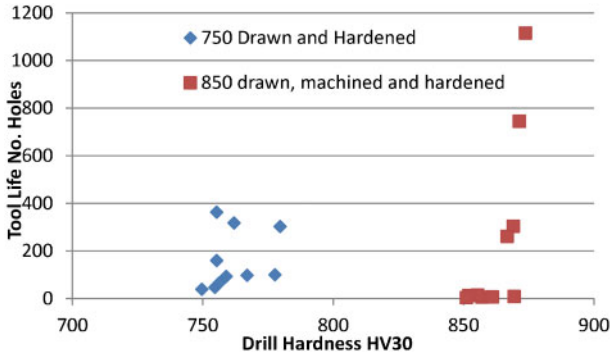

7 750 HV30 (group 1) and 850 HV30 (group 2) hardness verses number of holes to failure in accelerated drill testing on P20

failures may have resulted from defects in the microstructure developed in the drawing process. In the metallographic examination of the drill blanks it became evident that a number of the large primary carbides had fractured during drawing as shown in Fig. 6*c*. Similar observations of fracture of large primary carbides during the drawing process were reported by Yanagisawa *et al.*[6] Clearly, if such fractured primary carbides are located in the vicinity of the cutting edge then, under the probable built up edge cutting regime likely to occur with small diameter drills in the P 20 cold work tool steel, there is a high probability of brittle chipping of the cutting edge followed by rapid over heating of the outer corner and failure. Such a scenario is less probable in the softer group 1 drills since they are tough and therefore more tolerant to the defects generated in the drills. The fact that they are softer inevitably means that they wear more quickly by classical adhesive wear mechanisms.

Conclusions

Conclusions arising from the investigation are summarised as follows.

1. The poor hardening response of small diameter M35 HSS drills correlated with a reduction in carbon content of the drills following VHT.

2. It was established that high carbon levels and hence good hardening response could be achieved by removing up to 200 μm off the diameter of the HSS blanks. With the greatest improvement in carbon retention occurring in the first 50 μm off diameter. Metallographic examination revealed that this distance correlated with the thickness of an oxide scale on the blanks.

3. The presence and thickness of the oxide scale suggests that it is setting up a chemical diffusion gradient leading to rapid grain boundary diffusion of carbon during VHT. The problem is more evident in VHT rather than salt heat treatment because of the much longer times spent at temperatures above 1000°C during the hardening cycle.

4. Accelerated drill testing showed that under hard drills had a poor tool life but with a lower variance. Whereas the fully hardened drills had a higher variance in tool life due largely to several early life failures. Metallographic examination revealed that the latter could be due to the presence of defects in the form of large primary carbides which fractured in the drawing process.

Acknowledgements

The authors acknowledge the support of the CEO and Directors of Sutton Tools and acknowledge and thank Dr S. Dowey, Mr J. Toton and Dr B. Wood for their assistance and helpful discussion. A. Rousseau acknowledges the financial support of the Defence Materials Technology Centre. The authors also acknowledge the provision of facilities by, and the scientific and technical assistance of, the Australian Microscopy & Microanalysis Research Facility at the RMIT Microscopy & Microanalysis Facility, at RMIT University. This paper is based on a presentation at the 9th Tooling Conference/4th International Conference on Heat Treatment of Tools and Dies, organised by IFHTSE in Leoben, Austria on 11–14 September 2012.

References

1. C. S. Gonçalves, A. Slaviero, R. Mesquita, A. Tschiptschin and P. Haddad: 'Effect of cooling rate during quenching on the toughness of high speed steels', *J. ASTM Int.*, 2011, **8**, 4.
2. A. I. Lyapunov: 'Heat treatment of tools in vacuum', *Metal Sci. Heat Treat.*, 2001, **43**, (11–12), 429–430.
3. 'Steel and iron – determination of total carbon content', in 'Infrared absorption method after combustion in an induction furnace', EN ISO 9556:198, 2–11; 2001, Brussels, Comité Eurpoéen de Normalisation.
4. G. Hoyle (ed.): 'High speed steel'; 1988, Cambridge, Butterworths.
5. G. Dexter: 'Salt bath vs. vacuum furnace hardening of M2 high speed and D2 tool steel', 1996.
6. T. Yanagisawa, K. Sudo, H. Mizuno and S. Abeyama: 'The effect of cold drawing on the hardening and tempering hardness of tool steels', *Denki Seiko (Electr. Furn. Steel)*, 1986, **57**, (3), 170–180.

Chapter 3. Carbon Evolution during Vacuum Heat Treatment of High Speed Steel [130]

Vacuum 124 (2016) 85–88

Contents lists available at ScienceDirect

Vacuum

journal homepage: www.elsevier.com/locate/vacuum

Short communication

Carbon evolution during vacuum heat treatment of High Speed Steel

A.F. Rousseau [a, c, *], J.G. Partridge [a], Y.M. Gözükara [b], S. Gulizia [b], D.G. McCulloch [a]

[a] School of Applied Sciences, RMIT University, GPO Box 2476, Melbourne, VIC 3001, Australia
[b] CSIRO Manufacturing Flagship, Private Bag 10, Clayton South, VIC 3169, Australia
[c] Sutton Tools Pty. Ltd., 378 Settlement Road, Thomastown, VIC 3074, Australia

ARTICLE INFO

Article history:
Received 9 October 2015
Received in revised form
12 October 2015
Accepted 24 November 2015
Available online 27 November 2015

Keywords:
High speed steel
M35
Vacuum heat treatment
Evolved gas analysis

ABSTRACT

We report on the hardness response of vacuum heat treated (VHT) M35 HSS as a function of the thickness of oxide present during VHT. An almost linear relationship existed between the hardening response post-VHT and the oxide thickness pre-VHT. A similar relationship existed between the thickness of oxide pre-VHT and the carbon content post-VHT. CO evolution during VHT was observed from ~800 °C. In combination, these measurements show that CO evolution and carbon loss are increased in M35 HSS covered with surface oxide whilst hardening response is reduced. A full hardening response and unchanged carbon content were measured in M35 HSS VHT with surface oxide removed.

High Speed Steel (HSS) is a complex alloy tool steel accounting for over 30% of the global cutting tool market. In precision cutting tool fabrication, heat treatment of HSS in vacuum is increasingly preferred over heat treatment in salt. In both cases, correct heat treatment is vital to the performance of HSS cutting tools [1,2]. Typically, VHT includes several preheat, high heat, quenching and tempering stages. These stages are designed to produce a microstructure consisting of relatively large primary carbides in a tempered martensitic matrix, hardened by the precipitation of nano-scale secondary carbides [3]. Maintaining the high carbon content in the HSS throughout the VHT process is essential for the formation of these secondary carbides and the desired hardening response.

In the fabrication of HSS cutting tools, the HSS is generally supplied by the steel maker in the form of hot rolled coil. This inevitably means that the coil has a relatively thick oxide scale. At the cutting tool manufacturing plant, the oxidised coil is subject to cold drawing operations prior to VHT. Authors have previously reported on a correlation between the presence of surface oxide and decarburisation in hot working [4–8] and in powder metallurgy fabrication [9]. More recently, Rousseau et al. [10] reported on a correlation between hardening response of HSS and the presence of surface oxide on VHT heat treated HSS blanks. However, carbon evolution during VHT was not measured directly.

This paper describes an investigation into the VHT hardening response of oxidised M35 HSS. Differential scanning calorimetry (DSC) and evolved gas analysis (EGA) were combined with microstructural analysis and revealed the effects of surface oxide on the composition and microstructure of the VHT HSS. The relationship between the post VHT hardness and the thickness of oxide present during VHT was studied using Hardness Rockwell C (HRC) measurements.

In all experiments, the as-received composition (in at. wt %) of the M35 HSS was C 0.91%, Si 0.61%, Mn 0.28%, Cr 4.7%, Mo 4.56%, V 1.63%, W 5.8% and Co 4.12% and Fe balance. This material (with 6.2 mm diameter) had received one cold draw and was cut to 60 mm lengths. Ten sets of five samples of this material were centreless ground in 0.01 mm increments from 6.2 mm down to 6.1 mm diameter using a Royal Master TG Centreless Grinder with high flow flute grinding oil. The samples were then loaded in an Abar Ipsen cold wall vacuum furnace with a capacity for high pressure gas quenching up to 6×10^5 Pa, pumped down to 4.5 Pa and back-filled with nitrogen gas to 2×10^5 Pa. Convection heating was commenced with pre-heat steps of 550 °C for 120 min, 850 °C for 90 min and 1050 °C for 50 min. The chamber was then pumped down to 13×10^{-2} Pa and continued with radiant heating to 1190 °C. The austenitizing temperature of 1190 °C was held for 3 min and then quenched in nitrogen at 5×10^5 Pa down to 43 °C. Three tempers were completed at 550 °C and 2×10^5 Pa for

* Corresponding author. School of Applied Sciences, RMIT University, GPO Box 2476, Melbourne, VIC 3001, Australia.
E-mail address: andre-rousseau@hotmail.com (A.F. Rousseau).

http://dx.doi.org/10.1016/j.vacuum.2015.11.019
0042-207X/

180 min.

Metallographic analysis was conducted on selected HSS blanks before and after vacuum heat treatment. The selected HSS blanks were cross-sectioned with an abrasive cut-off wheel using high flow coolant. Samples were longitudinally and transverse mounted in conductive phenolic resin and polished using diamond abrasive laps, finishing with 0–1 μm diamond on a napped cloth. Where appropriate, samples were etched in 4% nital. Imaging was performed using a FEI Nova Nano scanning electron microscope (SEM). X-ray diffraction (XRD) was conducted on surface oxide removed from an as-received M35 HSS sample and a ground sample (with surface oxide fully removed) using a Bruker D4 X-ray diffractometer. Graphite-monochromated Cu Kα radiation (λ = 1.5406 Å) is produced by this instrument. The potential and current were 40 kV and 35 mA. The 2θ scan range was 5–90°, the step size was 0.02° and the count rate was 0.3 s. The bulk carbon contents (at. wt. % averaged from five measurements) of each sample were measured before and after VHT by infrared absorption spectroscopy after combustion in an induction furnace [11], as reported previously [10]. After VHT, Hardness Rockwell C (HRC) measurements were performed using a Wilson 2000 system on all samples (with ten differing pre-VHT oxide thicknesses). These measurements were averaged from five sample measurements (corresponding to five measurements for each pre-VHT oxide thickness).

An unground surface oxide covered M35 HSS sample was analysed in a Netzsch STA 449 F1 Jupiter system which enabled thermogravimetry (TG) and differential scanning calorimetry (DSC) in vacuum, during heating. These measurements were performed under an Ar gas (99.999% purity) purge to minimise surface oxidation, with a ramp rate of 10 °C/min to a maximum temperature of 1200 °C. A 100 μL alumina crucible contained the sample during vacuum heating. Evolved gases in the atomic mass range of 2–44 atomic mass units (AMU) were detected by coupling the TG/DSC system to a Thermostar Pfeiffer mass spectrometer.

Fig. 1(a) shows a longitudinal section with the oxide visible in the upper portion of the image. The inset shows a fractured primary carbide (> 5 μm in length). This fracturing, associated with cold drawing, has been reported by Yanagisawa et al. [12] who attributed poor hardening response after VHT of HSS to the resulting micro-voids (also visible in Fig. 1(a) inset). Fig. 1(b) shows a well

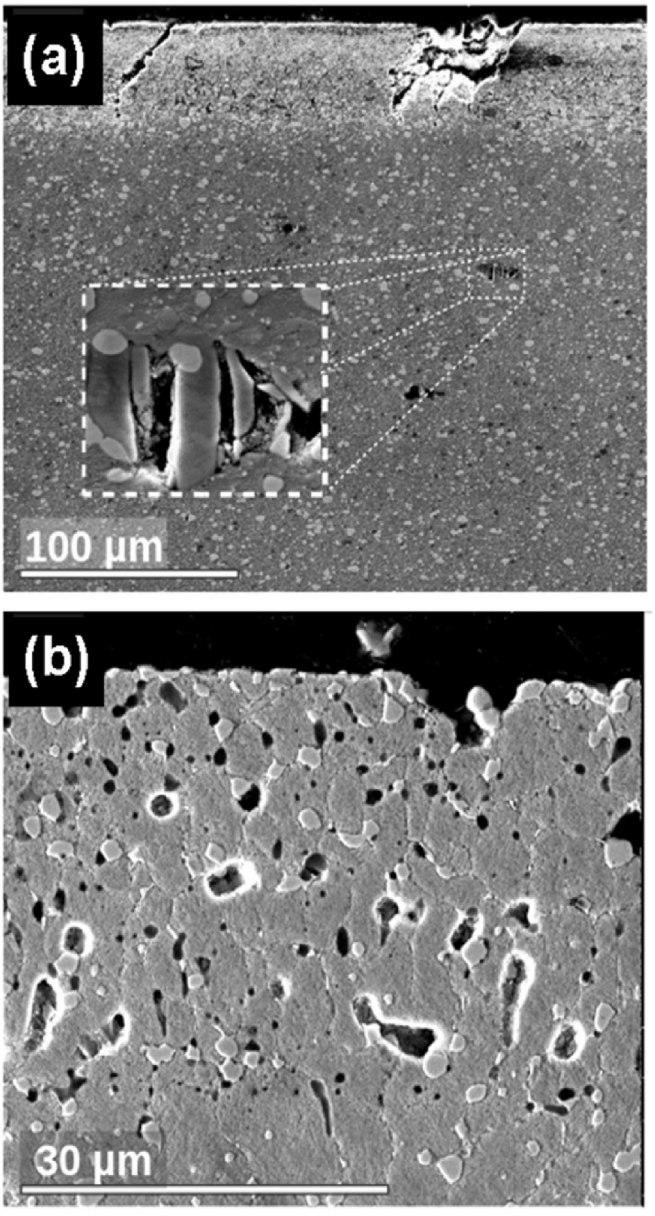

Fig. 1. Cross-sectioned M35 HSS (a) as-received and mounted longitudinally, and (b) after VHT and mounted transversely. The inset in (a) shows a large primary carbide fractured during cold drawing.

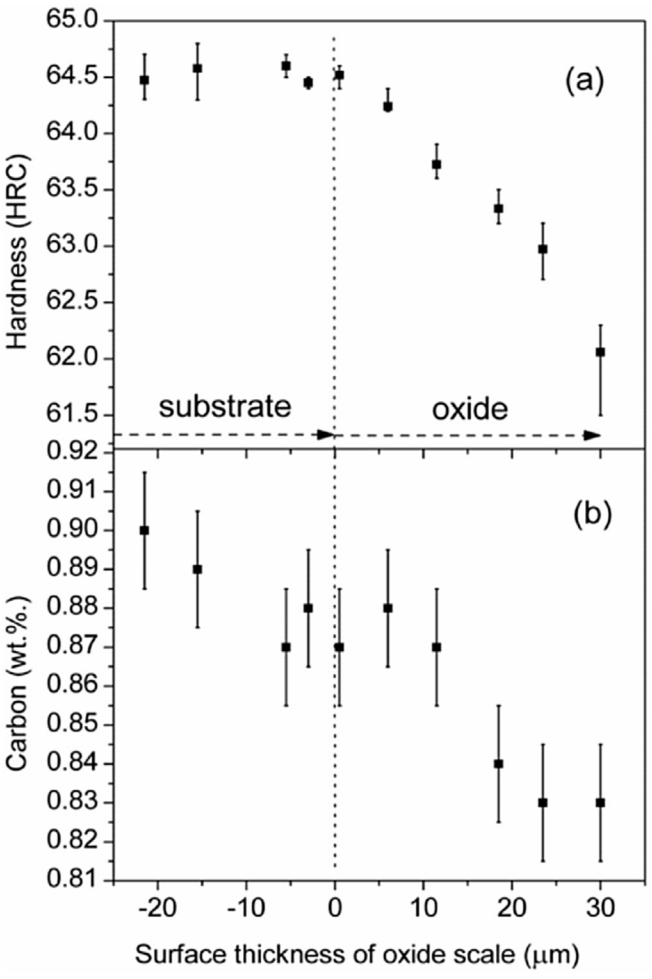

Fig. 2. (a) Hardness (HRC) and (b) carbon content measured as a function of incremental grind off the surface. Note: full hardness and full carbon content retention were achieved after 30 μm were ground from the surface. This result is consistent with full removal of the observed 30 μm (radial) oxide shown in Fig. 1(b).

adhered porous oxide (~30 μm in thickness) on a post VHT transverse section of the M35 HSS. X-ray diffractograms (not shown) were taken from the incrementally ground oxide and from the underlying M35 HSS. These showed that the oxide was composed mainly of Fe_20_3 and Fe_30_4 [6,13,14]. All peaks associated with iron oxides were absent from the diffractogram taken from the ground M35 HSS.

Fig. 2(a) reveals the relationship between the oxide thickness prior to VHT and the hardening response (HRC) after VHT. Samples with a pre-VHT surface oxide thickness of 30 μm exhibited only ~62 HRC and a bulk carbon content of only 0.83 wt. %. With decreasing pre-VHT oxide thickness, both the hardness and carbon content post VHT increased monotonically (Fig. 2(b)). In the samples with no surface oxide present pre-VHT, a hardening response of ~64.5 HRC and a carbon content of at least 0.87 wt. % were measured. Full hardness and full carbon content (0.90 wt. %) were only observed after grinding 15 μm into the M35 substrate. This effect is attributed to the surface roughening caused by the removal (grinding) of the oxide and due to the non-abrupt transition between the M35 and surface oxide (evident in Fig. 1(a)).

In Fig. 3(a), the TG curve shows the mass of a M35 HSS sample with oxide scale present during VHT. Significant mass reduction starts to occur just below 800 °C and a ~0.3% reduction is measured after heating to 1200 °C. The CO ion current measured from this sample is also shown in Fig. 3(a). From ~760 °C to ~880 °C, the evolved molecules were mainly CO with a significantly smaller fraction being CO_2, in agreement with previous reports [8].

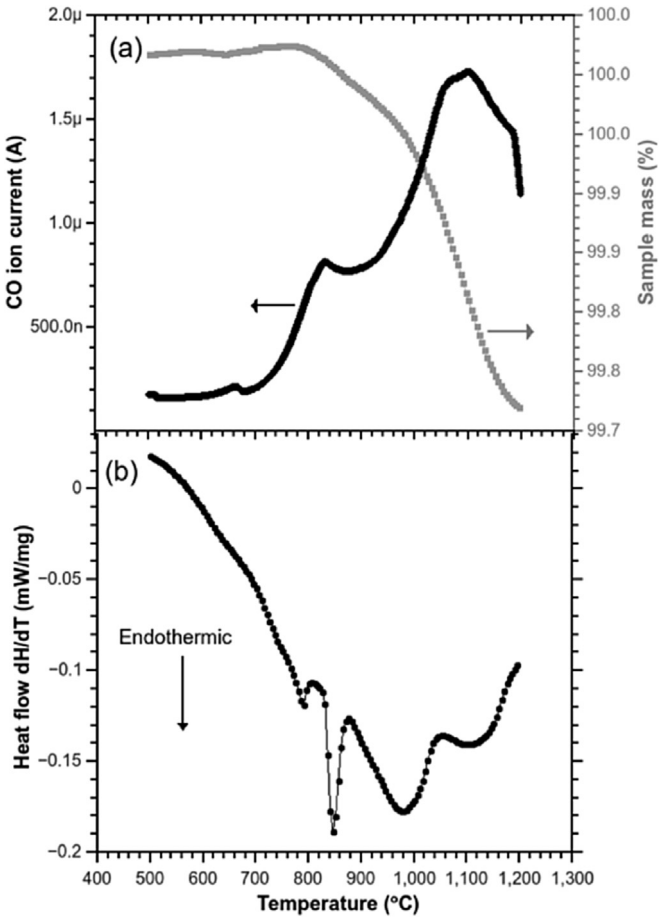

Fig. 3. (a) CO ion current and sample mass and (b) heat flow (dH/dT) versus sample temperature.

Between 780 °C and 810 °C, a transformation from $M_{23}C_6$ to M_7C_3 is known to occur [9]. Over this temperature interval, the evolution of CO increased, suggesting that carbon diffused from the $M_{23}C_6$to the substrate. From 960 to 1100 °C, CO continued to evolve, consistent with the dissociation of $M_{23}C_6$ (occurring between 900 and 1100 °C). Above 1100 °C, where the $M_{23}C_6$ was fully dissociated, the rate of CO evolution decreased. From 1150 °C to the solidus temperature (~1250 °C), M_6C began to dissociate, releasing more carbon [15,16].

Several endothermic peaks appear in the DSC measurements shown in Fig. 3(b). The first peak at 790 °C is associated with the Curie transformation temperature (Tc) [17]. The Ac_1 and Ac_3 transformation (BCC to FCC) occurs between 826 °C and 876 °C (in agreement with other work [18]), causing the second endothermic peak. Since carbon can move freely within the FCC austenite phase, above ~880 °C, mobile dissociated carbon is available to react with surface oxide [19]. This reduction process leads to the observed evolution of CO. Finally, the third and fourth endothermic peaks (occurring at 980 °C and 1100 °C) shown in Fig. 3(b) correspond respectively with the dissociation temperatures of M_6C_{23} and M_6C.

This paper reports on the hardness response achieved after VHT of M35 HSS as a function of the thickness of oxide present during VHT. Evolved gas analysis revealed CO evolution from ~800 °C which correlated with sample mass reduction, measured simultaneously by thermogravimetry. By removing the oxide incrementally and performing HRC measurements, an almost linear relationship between the hardening response and oxide thickness was observed. Infrared absorption mass spectrometry showed a similar relationship between the carbon content after VHT and the thickness of oxide present during VHT. With the oxide fully removed before VHT, a full hardening response and unchanged bulk carbon content were measured after VHT. This work illustrates the importance of surface preparation of HSS before VHT.

Acknowledgments

The authors thank Professor Edward Derry Doyle (RMIT), Sutton Tools Pty. Ltd. and the RMIT Microscopy & Microanalysis Facility.

References

[1] S. Söderberg, O. Vingsbo, M. Nissle, Performance and failure of high speed steel drills related to wear, Wear 75 (1982) 123–143.
[2] E.D. Doyle, Effect of different heat treatments on the wear of high speed steel cutting tools, Wear 27 (1974) 295–301.
[3] W. Rong, H.O. Andrén, H. Wisell, G.L. Dunlop, The role of alloy composition in the precipitation behaviour of high speed steels, Acta. Metall. Mater 40 (1992) 1727–1738.
[4] D.A. Teimer, A.G. Petrenko, L.A. Kurtova, Prevention of decarburization in the annealing of high-speed steel, Met. Sci. Heat Treat. Metals 2 (1960) 269–272.
[5] K. Sachs, C. Tuck, Surface oxidation of steel in industrial furnaces, J. Iron Steel Inst. 111 (1968) 1–17.
[6] A.M. Medvedev, E.A. Mazurenko, S.L. Vrochinskii, V.V. Nazarenko, A.G. Molyar, Protection of Steels and Alloys from Oxidation and Decarburization During Heat Treatment in Muffle and Bell Furnaces, Met. Sci. Heat Treat. Metals 45 (2003) 270–272.
[7] J. Zong, J. Yoon, Theoretical interpretation of the decarburization mechanism in convective oxygen steelmaking, Metall. Mater. Trans. B 21 (1990) 49–57.
[8] W.K. Jozwiak, E. Kaczmarek, T.P. Maniecki, W. Ignaczak, W. Maniukiewicz, Reduction behavior of iron oxides in hydrogen and carbon monoxide atmospheres, Appl. Catal. A-Gen 326 (2007) 17–27.
[9] S. Brust, Transformation of Surface Oxides during Vacuum Heat Treatment of a Powder Metallurgical Hot Work Tool Steel, Chalmers University of Technology, Gothenburg, 2013.
[10] A. Rousseau, E. Doyle, D. McCulloch, Vacuum heat treatment of high speed steel cutting tools, Int. Heat. Treat. Surf. Eng. 7 (2013) 110–114.
[11] EN ISO 9556:1989, Steel and Iron - Determination of total carbon content. (CEN), in: Infrared Absorption Method after Combustion in an Induction Furnace, CEN, Brussels, 2001, pp. 2–11.
[12] T. Yanagisawa, K. Sudo, H. Mizuno, S. Abeyama, The Effect of Cold Drawing on the Hardening and Tempering Hardness of Tool Steels, Electr. Furn. Steel 57 (1986) 170–180.

[13] W. Sun, A. Tieu, Z. Jiang, H. Zhu, C. Lu, Oxide scales growth of low-carbon steel at high temperatures, J. Mater. Process Tech. 155 (2004) 1300–1306.
[14] Q. Zhu, H.T. Zhu, A.K. Tieu, C. Kong, Three dimensional microstructure study of oxide scale formed on a high-speed steel by means of SEM, FIB and TEM, Corros. Sci. 53 (2011) 3603–3611.
[15] H. Wisell, An Experimental Study of Carbide/Austenite Equilibria in the High-Speed Steel Alloy System, Metall. Trans. A 22A (1991) 1391–1405.
[16] T. Malkiewicz, Z. Bojarski, J. Foryst, Carbides in Annealed and Quenched High Speed Steels, J. Iron Steel Inst. 193 (1959) 25.
[17] S. Raju, B.J. Ganesh, A. Banerjee, E. Mohandas, Characterisation of thermal stability and phase transformation energetics in tempered 9Cr–1Mo steel using drop and differential scanning calorimetry, Mater Sci. Eng. A 465 (2007) 29–37.
[18] A. Basu, B.K. Ghosh, S. Jana, S.C. Dasgupta, Effect of metallurgical variables on grain size of high-speed tool steels, Met. Technol, Lond 7 (1980) 151–158.
[19] R. Fruehan, The rate of reduction of iron oxides by carbon, Metall. Trans. B 8 (1977) 279–286.

Chapter 4. Microstructural and tribological characterisation of a nitriding/ TiAlN PVD coated duplex treatment applied to M2 High Speed Steel tools [122].

Surface & Coatings Technology 272 (2015) 403–408

Contents lists available at ScienceDirect

Surface & Coatings Technology

journal homepage: www.elsevier.com/locate/surfcoat

Microstructural and tribological characterisation of a nitriding/TiAlN PVD coating duplex treatment applied to M2 High Speed Steel tools

A.F. Rousseau [a,b,c,*], J.G. Partridge [a], E.L.H. Mayes [a], J.T. Toton [a,b,c], M. Kracica [a], D.G. McCulloch [a], E.D. Doyle [a,c]

[a] School of Applied Sciences, RMIT University, GPO Box 2476, Melbourne, VIC 3001, Australia
[b] Defence Materials Technology Centre, Level 2, 24 Wakefield Street, Hawthorn, VIC 3122, Australia
[c] Sutton Tools Pty. Ltd., 378 Settlement Road, Thomastown, VIC 3074, Australia

ARTICLE INFO

Article history:
Received 9 January 2015
Accepted in revised form 26 March 2015
Available online 1 April 2015

Keywords:
Plasma nitriding
TiAlN hard coating
Duplex treatment
X-ray diffraction
Drill testing
High speed steel

ABSTRACT

We describe a duplex nitriding and TiAlN coating process performed with no break in vacuum in an industrial scale deposition chamber. Plasma nitriding at 480 °C resulted in a fracture tough diffusion zone with no evidence of either a compound layer or grain boundary precipitation. Untreated, plasma-nitrided, coating-only and duplex-coated High Speed Steel (HSS) M2 coupons were microstructurally and mechanically characterised whilst similarly treated M2 ¼-inch jobber drills were subjected to accelerated drill testing (using D2 tool steel). In these tests, the duplex treated drills exhibited significantly improved wear performance and tool lives when compared with the other drills. After sectioning and electron microscopy, this extended tool life was attributed to increased toughness of the nitrided cutting edges coupled with improved adhesion at the substrate–TiAlN interface.

1. Introduction

Surface treatments have long been central to improvements in the performance of mechanical components and cutting tools. Amongst these, nitriding is a proven method for increasing the resistance of nitridable alloy steels to plastic deformation, fatigue and wear [1]. Traditionally it is conducted using a ferritic thermochemical method, in which nitrogen diffuses into a steel substrate when treated in an ammonia atmosphere at elevated temperatures (~520 °C). In plasma nitriding, nitrogen molecular gas is ionised in a glow discharge plasma to produce energetic nitrogen ions that enhance substrate diffusion [2]. Protective coating layers, typically composed of metal nitrides, carbides or carbonitrides and deposited by chemical vapour deposition (CVD) or physical vapour deposition (PVD), can also extend the capabilities of substrates. For example, in machining tools tribological interactions occurring at the chip–tool interface [3,4] are shown to be improved with the application of PVD coatings [5,6] however, these improvements are compromised if normal loading is sufficient to cause plastic deformation in the underlying substrate [7–10].

Duplex coatings, consisting of a nitrided steel substrate and a hard PVD coating, can exhibit the high hardness and high wear properties of PVD coatings combined with the enhanced fatigue resistance and load carrying properties of the nitrided substrate. The duplex coating process may be conducted sequentially using separate nitriding and coating apparatus or if it is suitably equipped, within the same vacuum chamber [8,11–16]. PVD equipment has been successfully adapted for plasma nitriding in order to duplex coat nitrided steel with CrAlN in a single, sequential process [7]. The resulting duplex coatings were shown (in scratch and impact fatigue tests) to have superior wear properties to those provided by CrAlN coatings on un-nitrided steel.

This paper reports the properties of M2 HSS coupons and test drills duplex treated by plasma nitriding combined with a commercial PVD TiAlN coating in a single vacuum system designed for industrial applications. TiAlN was selected as an outer coating layer as it is a proven ternary solid solution with good wear resistance, hardness, low friction and elevated operating temperature capability [17–21]. Microstructural analysis combined with mechanical/nano-indentation measurements and accelerated drill testing has been used to characterise the constituent layers and the duplex treatment as a whole.

2. Experimental methods

2.1. Nitriding

M2 HSS coupons (measuring 20 mm and 8 mm in diameter and thickness) and M2 ¼″ jobber drills were heat treated to achieve a nominal Vickers hardness (averaged from 5 indents per coupon) of 850HV30. Cleaning was performed in an alkaline solution with ultra-sonic agitation followed by rinsing in de-ionised water and drying at 110 °C. The tools were then loaded with vertical orientation onto a turntable (diameter 510 mm × 490 mm height) within the (800 mm × 900 mm × 900 mm)

* Corresponding author. Tel.: +61 490127988.
E-mail address: andre-rousseau@hotmail.com (A.F. Rousseau).

http://dx.doi.org/10.1016/j.surfcoat.2015.03.034
0257-8972/

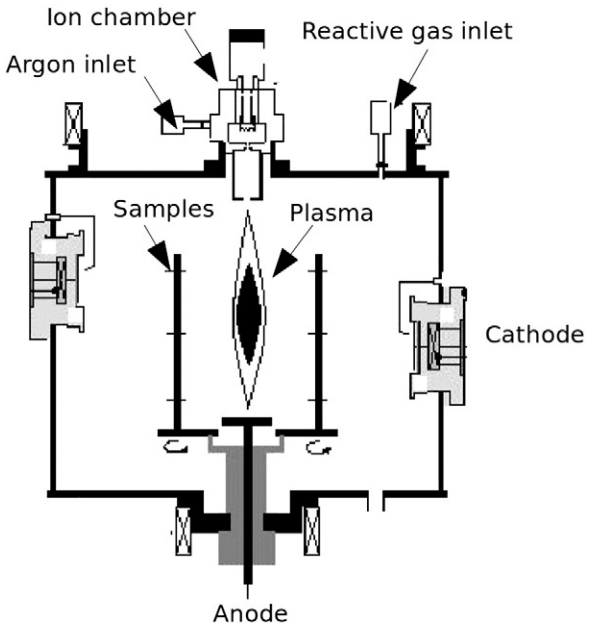

Fig. 1. Schematic of Balzers INNOVA industrial capacity cathodic arc PVD system.

chamber of an industrial capacity Balzers INNOVA cathodic arc PVD system, shown schematically in Fig. 1. The chamber was pumped down to 1×10^{-3} Pa before nitriding was performed in a 16:66:18 hydrogen:nitrogen:argon atmosphere at 1.0 Pa and 480 °C for 30 min. Combined radiative/electron-beam heating was used for nitriding and PVD coating. The plasma current was 150 A and the plasma potential was 58–63 V. A bias potential of −150 V was applied to the coupons and drills.

2.2. PVD coating

After nitriding and with no break in vacuum, argon etching was performed using a plasma current of 150 A and a bias of −170 V for 20 min at 0.25 Pa. The central plasma was then extinguished and the coating commenced at 450 °C in a three step process; (1) TiN functional layer (0.8 Pa, 100% N, bias −150 V and 2 Ti targets 180 A, 8 min), (2) TiAlN transition layer (3.2 Pa, 100% N, bias −40 V and 2 Ti targets 200 A plus 2 targets Ti/Al 200 A, 4 min), and (3) TiAlN top layer (3.2 Pa, 100% N, bias −40 V and 4 Ti/Al targets 200 A, 130 min). TiAlN coatings were deposited with a thickness of ~3 μm. TiN and Ti-rich interlayers were incorporated to reduce thermal and lattice mismatch at the substrate/coating interface [14,22].

2.3. Metallography

The nitrided and coated surfaces were imaged in a scanning electron microscope (SEM) and, topographically, using a Veeco Dimension 3100 atomic force microscope (AFM) operating in tapping mode with a <10 nm radius-of curvature Si tip. The coating thickness and nitriding diffusion depths were determined from coupons cross-sectioned with an abrasive cut-off wheel, mounted in a phenolic conductive resin and polished using diamond abrasive laps. The polished cross-sections were etched with 4% Nital for 25 s and then SEM imaged. A Bruker D4 X-ray diffractometer (fitted with graphite-monochromated Cu Kα radiation source (= 1.5406 Å) with a potential of 40 kV and a current of 35 mA) was used to obtain X-ray diffraction measurements (2θ scan range 5–90°, step size 0.02° and a count rate of 0.3 s) from the coatings and nitrided coupons. X-ray photoelectron spectroscopy (XPS) was performed using a Thermo Scientific K-Alpha system equipped with an Al Kα X-ray source (1486.7 eV), takeoff angle of 90°, pass energy of 50 eV and 400 μm diameter analysed area. These measurements revealed changes in chemical bonding occurring after plasma nitriding.

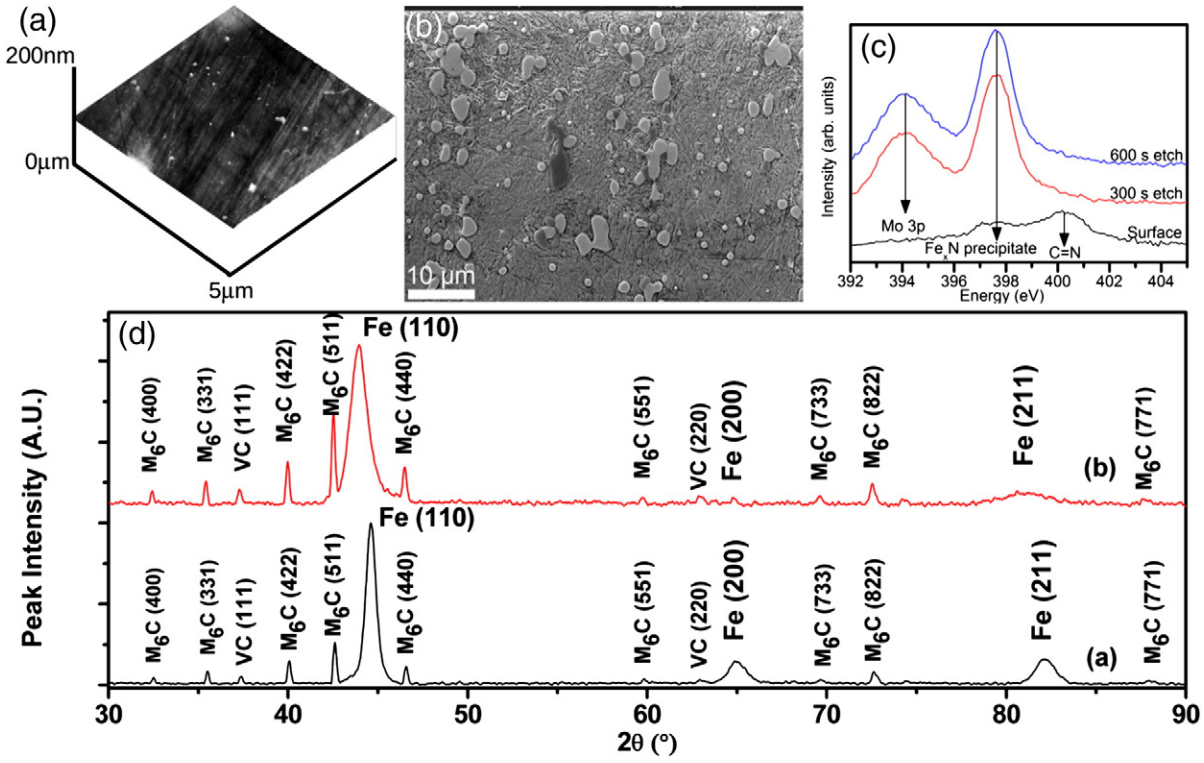

Fig. 2. (a) AFM topographical image, (b) cross-sectional SEM image, (c) XPS N 1s peak and (d) X-ray diffractograms (before and after bright nitriding) measured from a heat-treated and nitrided M2 coupon.

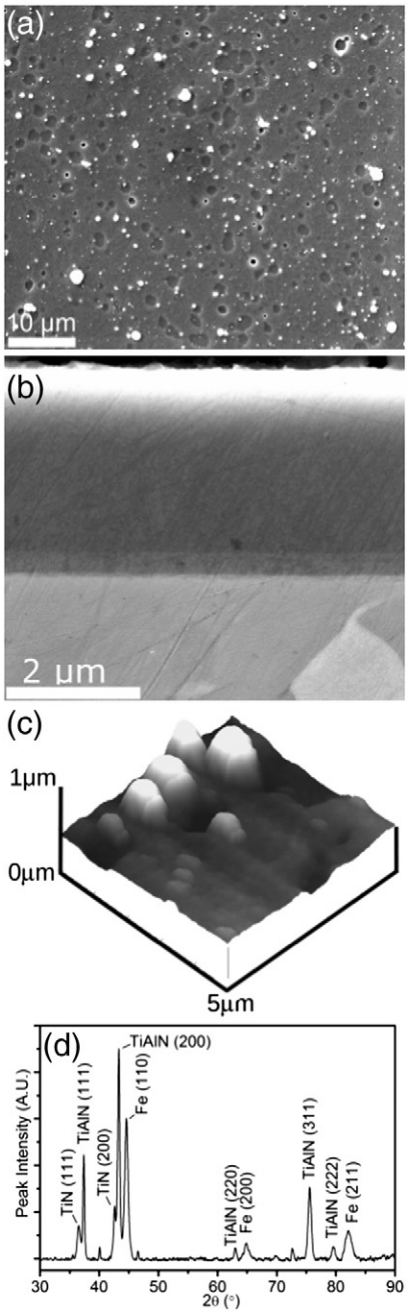

Fig. 3. (a) SEM plan view image, (b) cross-sectional SEM image, (c) AFM topographical image and (d) X-ray diffractogram taken from the TiAlN coating-only coupon.

2.4. Mechanical testing

Surface hardness (HV0.1) measurements were made on a Schimadzu Seisakusho Micro-Hardness Tester Type-M using a 100 g load for 15 s and taking an average from five indents. Hardness Rockwell C (HRC) indentation measurements were conducted to evaluate the coating adhesion according to the Verein Deutscher Ingenieure (VDI) guideline [23]. The mechanical properties of the TiAlN coatings were also studied using a Hysitron 950 Triboindenter fitted with a Berkovich indentation tip. To determine the hardness, H and effective elastic modulus (E^*), multiple indents were made with a maximum force of 10 mN. Hardness was calculated using the Oliver and Pharr method [24]. The maximum penetration depth was ~130 nm (<5% of coating thickness). Accelerated drill testing was conducted on a HAAS VF2 CNC milling centre. The substrate was D2 cold work tool steel (carbon 1.55 wt.%, chromium 12.0 wt.%, molybdenum 0.75 wt.%, vanadium 0.9 wt.%) with a cutting speed and feed of 35 m/min and 0.125 mm/rev. The blind hole depth was 2.5 times the diameter and hole locations were randomised over the drill plate to minimise effects due to plate inhomogeneity.

3. Results and discussion

3.1. Nitriding

Before performing the main set of nitriding/coating processes, M2 HSS coupons were plasma nitrided with different applied biases and their hardnesses were determined. A hardness exceeding 11 GPa was achieved after plasma nitriding using a moderate substrate bias of

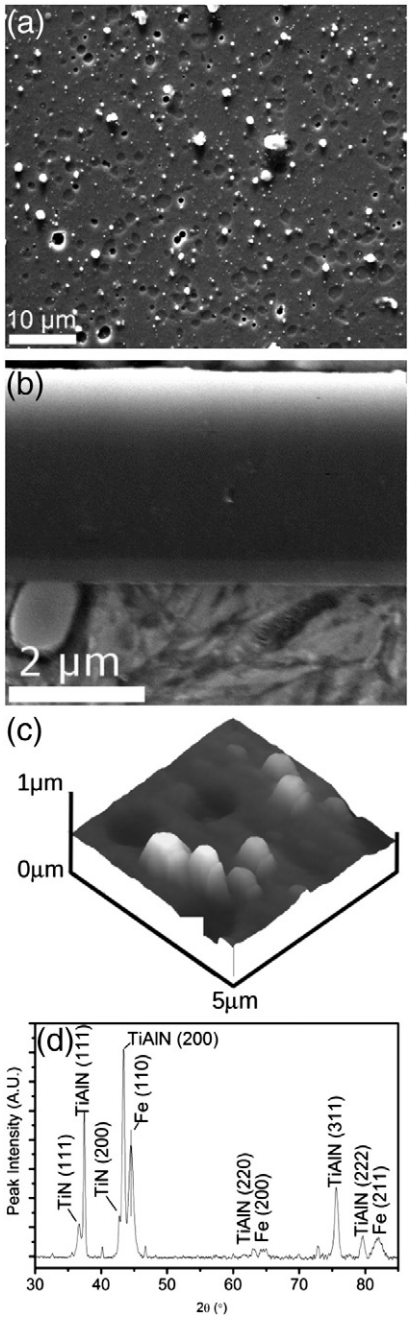

Fig. 4. (a) Plan view SEM image, (b) cross-sectional SEM image, (c) AFM topographical image and (d) X-ray diffractogram taken from the duplex nitrided/TiAlN coated coupon.

−150 V. This bias is considered sufficiently low to minimise 'edge effects' observed at higher biases [12,25,26]. Using a similar plasma, Muratore *et al.* showed that the magnitude and energy distribution of the ion flux changed significantly with distance from the plasma source [27]. The dependence of the nitrided hardness on position, relative to the central plasma, was therefore investigated. It was found that the reduction in hardness between coupons 170 mm and 230 mm from the central plasma during plasma nitriding (corresponding to the nearest and furthest locations provided by the rotating substrate holder) was less than 7%.

Fig. 2 shows microstructural measurements taken from a plasma nitrided M2 coupon. In Fig. 2(a), the surface topography (measured using AFM) is shown. The RMS roughness of this scanned surface is <5 nm. A cross-sectioned sample showing the diffusion zone post nitriding is shown in Fig. 2(b). The acicular microstructure extends to a depth of ~30 μm with no observed compound layer or grain boundary precipitation, typical of effectively nitrided HSS and consistent with a surface hardness of ~11 GPa (measured by nanoindentation). Fig. 2(c) shows the N1s XPS peak. The peak at ~397.4 eV can be attributed to Fe_xN precipitate. The peak at ~400.5 eV can be attributed to C═N [28]. The surface scan shows the presence of a C═N nitride. However, after etching, the only visible peak associated with a nitride is that from Fe_xN precipitate. Carbon present at the surface but absent at deeper etch levels is consistent with carbon diffusing to the stress free regions [12] and an effectively plasma nitrided M2 HSS substrate. X-ray diffractograms from heat treated coupons before and after nitriding are shown in Fig. 2(d). Peaks are indexed to the M_6C and MC primary carbides and to body centred cubic αFe. Peaks attributable to a compound layer [29] were not observed, indicating that the process parameters resulted in 'bright nitriding'. Whilst there is debate over whether a compound layer is detrimental within duplex coatings [7,12,13,30], the compound layer can decompose to produce a 'black' layer which reduces the bond strength between the coating and nitrided subsurface [8]. The peak associated with αFe shifts to a lower 2θ after nitriding, indicating an increased 'd' spacing which is consistent with a previous report [12] showing that nitriding increases the residual compressive stress in the diffusion zone. The αFe peak also broadens after nitriding. Similar broadening and peak shift have been observed previously and attributed to increases in uniform and non-uniform strain (precipitation of Cr_xN) [31,32].

3.2. Coating

Fig. 3 shows microstructural measurements and images taken from a heat treated TiAlN coating-only coupon (with no nitriding treatment). The SEM and AFM images (Fig. 3(a) and (c)) clearly show macro crevices and macro-particles on the surface which are typical in films deposited from an unfiltered cathodic arc. The RMS roughness of the 3.1 μm thick TiAlN coating was measured using AFM to be 71 nm, a typical value for standard (non-duplex) tool commercial coatings. The TiN interlayer between the TiAlN coating and nitrided M2 HSS steel can be seen in Fig. 3(b). The white and grey inclusions seen in the HSS are M_6C and MC primary carbides, respectively.

An X-ray diffractogram from the TiAlN film is shown in Fig. 3(d) with major peaks indexed to Fe, TiN and TiAlN. As reported by Mashiki *et al.* [33], the (111) and (200) peaks are present. The film exhibits slightly preferred (200) orientation which is consistent with the findings of Zhao *et al.* [34]. These authors found that during the initial stages of energetic TiN film growth (with moderate substrate bias), the (200) orientation dominated but as growth continued, the preferred orientation switched to (111).

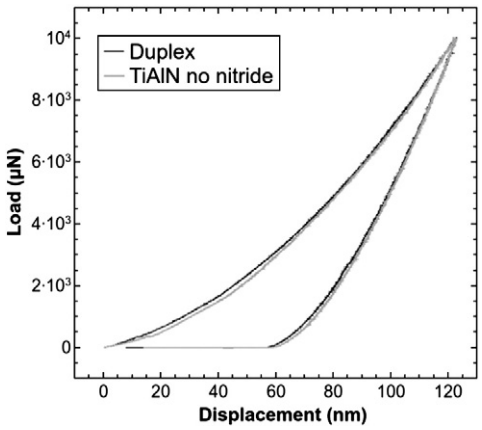

Fig. 6. Nano-indentation load–displacement curves measured from the TiAlN coating-only and TiAlN duplex treated M2 HSS coupons.

3.3. Duplex coating

Fig. 4 shows SEM images (Fig. 4(a) and (b)), an AFM image (Fig. 4(c)) and an X-ray diffractogram (Fig. 4(d)) taken from the duplex treated M2 coupon. The coating has very similar surface morphology (Fig. 4(a) and (b)) and microstructure (Fig. 4(d)) when compared with the coating deposited on the non-nitrided M2 coupon (shown in Fig. 3). As expected given the identical parameters used to deposit both coatings, the RMS roughnesses were also very similar (69 nm in the duplex coating versus 71 nm in the coating-only). The microstructure of the nitrided zone (Fig. 4(b)) in the duplex treated coupon closely

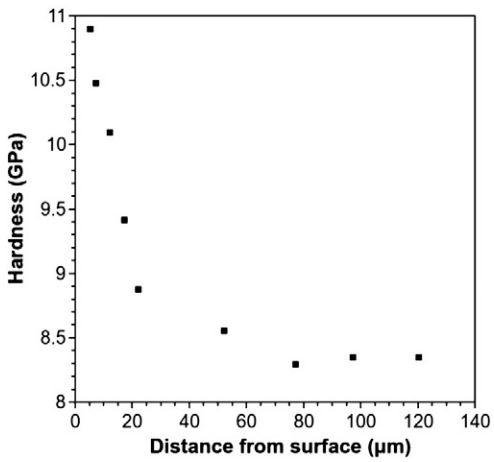

Fig. 5. Micro-hardness of a cross-sectioned nitrided M2 HSS coupon measured as a function of depth into the substrate.

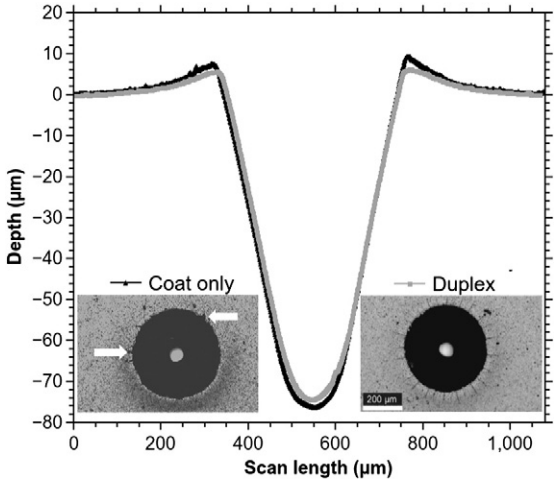

Fig. 7. Crater profiles and (inset) images taken from the TiAlN coating-only and TiAlN duplex treated M2 HSS coupons after Rockwell C indentation.

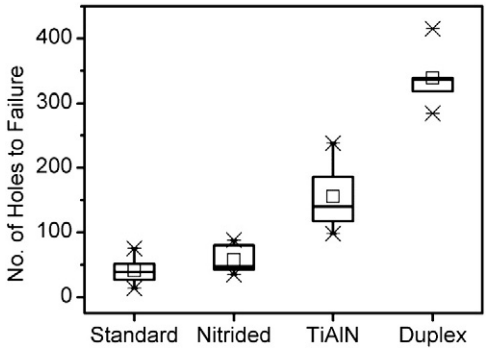

Fig. 8. Tool lifetimes of standard (untreated), nitrided, TiAlN coating-only and TiAlN duplex treated M2 HSS 1/4″ jobber drills.

resembled that of the M2 HSS coupon subjected to only the nitriding process (Fig. 2(b)). With these similarities verified, the mechanical characteristics of the heat-treated, nitrided, coated and duplex-coated M2 HSS were compared, as described in Section 3.4.

3.4. Mechanical testing

A hardness–depth profile taken from a cross-sectioned duplex treated M2 coupon is shown in Fig. 5. This shows a typical hardening response (up to ~11 GPa) to a depth of ~40 μm. Nano-indentation was performed in order to assess the hardness of the TiAlN coating (Fig. 6). This showed the hardness of the TiAlN to be independent of the treatment of the underlying coupon and equal to ~30 GPa, in agreement with previous measurements [35].

Rockwell C indentation tests as per VDI standard 3198 (with an ultimate load of 150 kg), resulted in the craters shown as insets in Fig. 7. The depth profiles of the craters on the coated and duplex treated coupons are shown in the main plot in Fig. 7 and show the increased plastic deformation occurring in the non-nitrided M2 substrate. Increased delamination around the crater is also evident in this sample and highlighted with arrows in the inset image. The VDI test is a qualitative test in which adhesion is ranked from HF (Haftfestigkeit) HF1 to HF6. Rankings from 1HF to 4HF are typically considered acceptable for standard tooling applications. When considering the inset images in Fig. 7, both samples exhibit radial cracking consistent with plastic deformation so are considered to be between HF 1 and HF 2 [36].

The box and whisker plot (showing median number of drilled holes and the 25% and 75% quartile positions) in Fig. 8 shows the tool lifetimes of untreated, nitrided, TiAlN coating-only and duplex treated jobber drills. There are significant differences in operational lifetime (number of holes drilled before failure) between the nitrided, PVD TiAlN coating-only and duplex treated drills. Comparing the latter two treatments, the median tool lifetime of the duplex treated drills is more than twice that of the TiAlN coating-only drills.

Fig. 9 shows SEM images taken at the outer corner of the duplex and TiAlN coating-only drills, cross-sectioned after testing to failure. Fig. 9(a) shows the duplex drill with a worn but intact TiAlN coating on its rake face. The worn flank extending horizontally from the cutting edge is approximately 70 μm in length. In this drill, shown in greater detail in Fig. 9(b), there is no evidence of deformation in the underlying

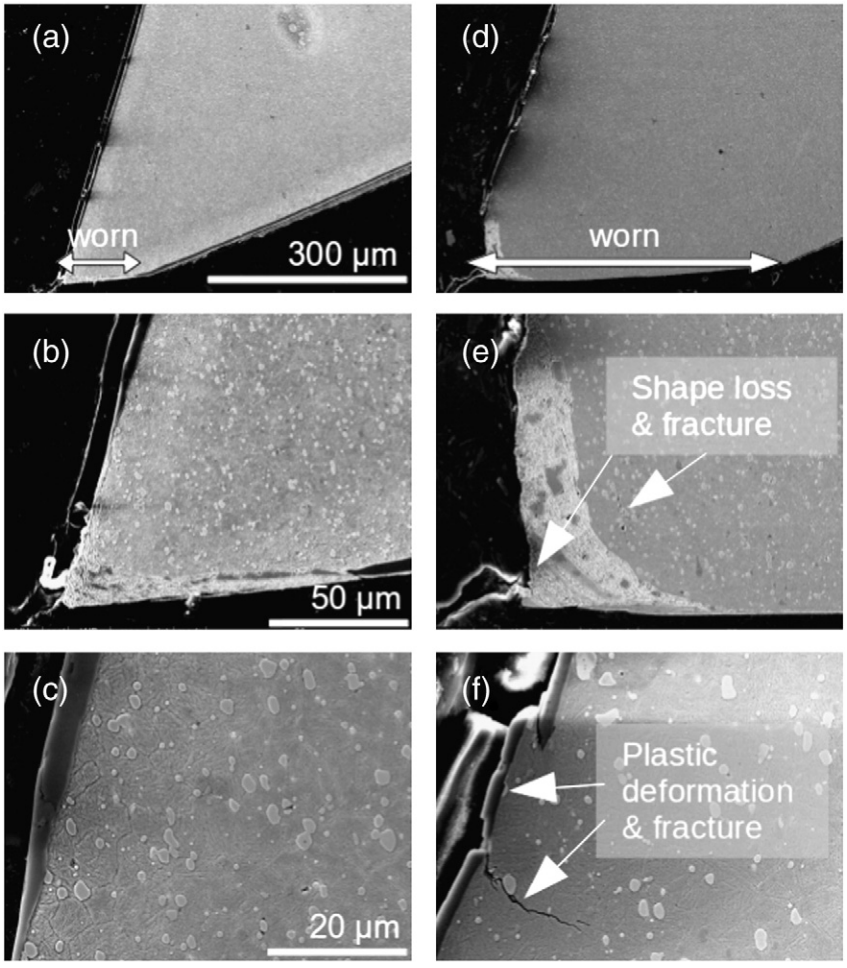

Fig. 9. SEM images of (a–c) duplex treated and (e–f) TiAlN coating-only drills cross-sectioned after testing to failure. Annotation highlights wear, deformation and fracture. In each row, scale bars are common to both images.

nitrided substrate. The D2 cold worked tool steel seen adhered to the drill indicates that the built up edge (BUE) wear mechanism proposed by Trent [37,38] occurred during the accelerated drill testing. The TiAlN coating-only drill (Fig. 9(d)) exhibits greater wear, with complete removal of the coating, a severely increased cutting edge radius and a longer wear flank region (>300 μm) extending horizontally from the cutting edge. Again, adhered D2 is visible on the cutting edge, consistent with the BUE wear mechanism. Fig. 9(e) shows the rake face at the outer corner and the formation of a wear land on the flank. This is revealed in greater detail in Fig. 9(f) which also shows areas on the rake face that have succumbed to plastic deformation. By contrast, the comparable images of the duplex treated drill (Fig. 9(b) and (c)) show no significant deformation and no signs of fracture. These characteristics are consistent with the claimed benefits of duplex coating, that is, the nitrided (hardened) and coated substrate is less prone to the plastic deformation and resulting delamination that occur in non-nitrided but similarly coated substrates [12,13].

4. Conclusions

Duplex treatments enable low friction PVD coatings to be combined with a nitrided substrate for improved support. In this work, the operational lifetimes of PVD coated, nitrided and duplex treated M2 HSS drills were compared. Within a single cycle duplex process (with no break in vacuum), low pressure, low voltage plasma nitriding resulted in a fracture tough diffusion zone in the M2 HSS with no evidence of a compound layer or grain boundary precipitation. Cathodic arc deposited TiAlN served as the PVD coating, with interlayers incorporated to effectively reduce substrate/coating property mismatches. In accelerated drill testing, the duplex treated drills provided more than double the median tool life of drills prepared similarly but with the TiAlN coating-only. Electron microscopy conducted after drill testing to failure revealed extensive plastic deformation and delamination on the cross-sectioned TiAlN coating-only drill. By contrast, plastic deformation was not discernible in the cross-sectioned duplex treated drill and delamination was significantly reduced. These results are consistent with the claimed benefits of duplex treatments and show that an industrial scale, single cycle process can be used to improve the wear performance and operational lifetimes of HSS drills.

Acknowledgements

The authors thank Dr Stephen J. Dowey, the DMTC (Defence Materials Technology Centre), established and supported by the Australian Government's Defence Future Capability Technology Centre (DFCTC), Sutton Tools Pty. Ltd. and the RMIT Microscopy & Microanalysis Facility.

References

[1] M.A. Pessin, M.D. Tier, T.R. Strohaecker, A. Bloyce, Y. Sun, T. Bell, Tribol. Lett. 8 (2000) 223–228.
[2] D. Pye, Practical Nitriding and Ferritic Nitrocarburizing, first ed. ASM International, Materials Park, OH, 44073-0002, USA, 2003.
[3] E.D. Doyle, J.G. Horne, D. Tabor, Proc. R. Soc. Lond. Ser. A 366 (1979) 173–183.
[4] E.D. Doyle, S. Dowey, Mater. Sci. Forum 618 (2009) 117–126.
[5] E. Doyle, Y. Wong, T. Quang, S. Dowey, Int. Heat Treat. Surf. Eng. 3 (2009) 165–170.
[6] A. Leyland, A. Matthews, Surf. Coat. Technol. 177 (2004) 317–324.
[7] S. Yang, K. Cooke, H. Sun, X. Li, K. Lin, H. Dong, Surf. Coat. Technol. 236 (2013) 2–7.
[8] T. Bell, H. Dong, Y. Sun, Tribol. Int. 31 (1998) 127–137.
[9] Y. Sun, T. Bell, Mater. Sci. Eng. 140 (1991) 419–434.
[10] J.C.A. Batista, M.C. Joseph, C. Godoy, A. Matthews, Wear 249 (2001) 971–979.
[11] F. Sanchette, E. Damond, M. Buvron, L. Henry, P. Jacquot, N. Randall, P. Alers, Surf. Coat. Technol. 94–95 (1997) 261–267.
[12] C. Kwietniewski, W. Fontana, C. Moraes, A.D.S. Rocha, T. Hirsch, A. Reguly, Surf. Coat. Technol. 179 (2004) 27–32.
[13] T. Sato, K. Sugai, S. Ueda, K. Matsunami, M. Yasuoka, Surf. Coat. Technol. 169 (2003) 45–48.
[14] P. Saikia, A. Joseph, R. Rane, B.K. Saikia, S. Mukherjee, J. Theor. Appl. Phys. 7 (2013) 1–12.
[15] T. Michler, M. Grischke, K. Bewilogua, H. Dimigen, Thin Solid Films 322 (1998) 206–212.
[16] B. Navinšek, P. Panjan, F. Gorenjak, Surf. Coat. Technol. 137 (2001) 255–264.
[17] A. Hörling, L. Hultman, M. Odén, J. Sjölén, L. Karlsson, Surf. Coat. Technol. 191 (2005) 384–392.
[18] P.C. Jindal, A.T. Santhanam, U. Schleinkofer, A.F. Shuster, Int. J. Refract. Met. Hard Mater. 17 (1999) 163–170.
[19] P. Hedenqvist, S. Jacobson, S. Hogmark, Surf. Coat. Technol. 97 (1997) 656–660.
[20] E.J. Bienk, H. Reitz, N.J. Mikkelsen, Surf. Coat. Technol. 76–77 (1995) 475–480.
[21] M. Kawate, A.K. Hashimoto, T. Suzuki, Surf. Coat. Technol. 165 (2003) 163–167.
[22] J. Gunnars, U. Wiklund, Mater. Sci. Eng. 336 (2002) 7–21.
[23] D.-B.A. Test, Richlinie, 31981992. 7.
[24] W.C. Oliver, G.M. Pharr, J. Mater. Res. 19 (2004) 3–20.
[25] C. Muratore, D. Leonhardt, S.G. Walton, D.D. Blackwell, R.F. Fernsler, R.A. Meger, Surf. Coat. Technol. 191 (2005) 255–262.
[26] G. Nayal, D. Lewis, M. Lembke, W.-D. Münz, J. Cockrem, Surf. Coat. Technol. 111 (1999) 148–157.
[27] C. Muratore, S. Walton, D. Leonhardt, R. Fernsler, D. Blackwell, R. Meger, J. Vac. Sci. Technol. A 22 (2004) 1530–1535.
[28] A. Laskarakis, S. Logothetidis, C. Charitidis, M. Gioti, Y. Panayiotatos, M. Handrea, W. Kautek, Diam. Relat. Mater. 10 (2001) 1179–1184.
[29] A. da Silva Rocha, T. Strohaecker, V. Tomala, T. Hirsch, Surf. Coat. Technol. 115 (1999) 24–31.
[30] A. Nishimoto, H. Nii, R. Narita, K. Akamatsu, Surf. Coat. Technol. 228 (2012) S558–S562.
[31] B.D. Cullity, S.R. Stock, Elements of X-ray Diffraction, first ed. Prentice Hall Upper Saddle River, NJ, 2001.
[32] P. Withers, H. Bhadeshia, Mater. Sci. Technol. Ser. 17 (2001) 355–365.
[33] T. Mashiki, H. Hikosaka, H. Tanoue, H. Takikawa, Y. Hasegawa, M. Taki, M. Kumagai, M. Kamiya, Thin Solid Films 516 (2008) 6650–6654.
[34] J. Zhao, X. Wang, Z. Chen, S. Yang, T. Shi, X. Liu, J. Theor. Appl. Phys. 30 (1997) 5.
[35] R. Rodriguez-Baracaldo, J. Benito, E. Puchi-Cabrera, M. Staia, Wear 262 (2007) 380–389.
[36] P.C. Jindal, D.T. Quinto, G.J. Wolfe, Thin Solid Films 154 (1987) 361–375.
[37] E.M. Trent, Wear 128 (1988) 47–64.
[38] E.M. Trent, Wear 128 (1988) 29–45.

Chapter 5. Discussion, Conclusions and Further Work

This chapter discusses the research findings presented in chapters 2-4. The following sub-sections summarise the findings of the three papers individually, before collating them and drawing conclusions on the body of work as a whole. All aspects of the project work are discussed with reference to and in the context of previously published work and contributions to the wider field are highlighted. Finally, conclusions are drawn and avenues for further work are suggested.

5.1 VHT of HSS Cutting Tools

As in many manufacturing industries, controlling variability is of critical importance to the producers of high performance cutting tools. Prompted by the variations observed in vacuum hardened small diameter cutting tools (< 5.0mm), the work described in chapter 2 was performed to isolate the conditions required in VHT to provide optimum hardening of HSS tools less than 5 mm in diameter. Smaller diameter tool blanks, having less mass, should quench more rapidly thus promoting a good hardening response [45]. Cold drawing leads to work hardening through high strain deformation [13]. Each cold draw process required a sub-critical interstage anneal [33]. Incorrect atmosphere during annealing can cause carbon loss leading to a poor hardening response in VHT [53, 131]. While sub-critical annealing was initially considered to be the primary cause, bulk carbon content testing after annealing and prior to VHT showed normal values of ~0.9 wt. % carbon, while post VHT bulk carbon content resulted in lower carbon content. A relationship between the number of draws and reducing carbon content post-VHT was established. As discussed previously, carbon is the primary constituent element for hardening response in heat treatment [26]. It was found from drawing, while the material diameter reduced, the surface oxide thickness remained unchanged. The smaller the diameter, the greater the loss of carbon observed. Bulk carbon content and hardness testing post-VHT confirmed this. Removing the surface oxide prior to VHT revealed carbon loss reduced and full optimised hardening response in post-VHT was restored. A correlation between carbon loss and hardening response in VHT in accelerated drill testing was established. The correlation between carbon loss and surface oxide was therefore considered the next step in the investigation since performance of cutting tools was the primary focus for the thesis.

5.2 Carbon Evolution during VHT of HSS

In chapter 3, the relationship between surface oxide, carbon loss and post-VHT hardness was explored in greater detail. In particular, gas evolved during VHT was analysed to determine whether it contained carbon. Again, the bulk carbon content and hardness of HSS samples were measured post-VHT. Incremental removal of the surface oxide (determined to be composed mainly of Fe_2O_3 and Fe_3O_4) enabled the hardness and carbon content to be compared with the thickness of surface oxide present before VHT. A clear trend was observed; lower carbon content and hardness was measured in samples undergoing VHT with thick surface oxide layers present. Full hardness and ~0.9 wt. % carbon content were measured in samples that underwent VHT with no surface oxide present. The evolved gas from the sample was found to contain CO as the temperature exceeded 800 ℃, coinciding with an increased rate of sample mass loss. At this temperature, the primary carbides begin to dissociate, releasing mobile carbon into the bulk. With the surface oxide removed, optimal hardening response of HSS in VHT allowed the work on improving cutting tool performance from standard and leads to the work in chapter 4.

5.3 Duplex treatment of HSS tools for prolonged operational life

Chapter 4 describes an industrially implementable duplex process for improving the performance of HSS twist drills. In this duplex process, a plasma nitriding stage is followed by PVD coating of ~3μm TiAlN in a single cycle i.e. with no break in vacuum. The plasma nitrided diffusion zone of the HSS substrate was characterized using XRD and XPS. Characterization of the PVD coating surface between coating-only and duplex cutting tools using various techniques indicated that both were similar in adhesion so no performance gain could be attributed other than nitriding before PVD coating. Accelerated drill testing showed the median life of duplex treated twist drills was more than twice that of TiAlN coated-only twist drills consistent with a hard but fracture tough substrate and excellent PVD coating adhesion. Plasma nitriding improved the substrate hardness resulting in less plastic deformation during cutting and improved support of the PVD coating. This is relevant to

industry as there was significant improvement in HSS cutting tool performance with low impact on process cycle times.

5.4 Summary

The investigations described in chapters 2-4 are spread over the full manufacturing process, from the as-received coil to the completed tool. They were driven by industrial requirements for reduced variability and improved performance/lifetime. Performance was quantified by measuring the rate of material removal in accelerated drill testing. Metallurgy was revealed using a suite of structural and chemical analysis described in chapters 2-4.

Variation in hardening response experienced post-VHT on small diameter HSS blanks was attributed to loss of carbon from the material. As-received HSS coil was drawn to various sizes as part of the tool manufacturing process with a sub-critical anneal employed between each subsequent draw. Two lines of investigation were embarked upon to elucidate to poor hardening after VHT. It has been reported that high strain deformation during drawing causes the fracture of large primary carbides (<5 μm) [7, 132] leading to micro-voids and consequently poor hardening response after VHT. The first line of investigation was to investigate the effects of high strain deformation on hardening response of HSS after VHT. The second was a loss of atmospheric control during annealing and/or VHT. While fractured primary carbides were observed, bulk carbon testing revealed that a loss of carbon occurred during VHT. The smaller the draw size, the greater the loss of carbon post-VHT. The surface oxide on the as-received HSS coil was observed to survive through the drawing process however, when removed, the HSS bulk carbon content returned to the as-received condition of ~0.9 wt. % carbon and a normal hardening response in VHT was observed. To observe the effects of poor hardening response in cutting conditions, accelerated drill testing was conducted.

This revealed that poor hardening in VHT resulted in a lower median life while correct hardening resulted in a better tool life. Notwithstanding, the correct hardening response also yielded some early life failures in accelerated drill testing which was attributed to broken primary carbides on the cutting

edge due to the HSS being more brittle compared with the poor hardening response tool while being softer were tougher [2-4, 34, 36, 133].

To better understand loss of carbon of HSS in VHT, a refined series of tests were conducted. HSS M35 6.2 mm as-received and one draw (no anneal) blanks were ground in 0.01 mm increments to 6.1 mm. Post-VHT hardness testing revealed an almost linear relationship between hardness and surface oxide thickness and similarly between surface oxide thickness and bulk carbon content. XRD showed the surface oxide was predominantly Fe_2O_3 and Fe_3O_4. M35 HSS samples with the surface oxide in the as-received condition were analysed using EGA coupled with DTA and TG during a VHT cycle. EGA revealed that CO was the predominant species. While the fracture of large primary carbides was observed, the surface oxide was found to be the predominant cause of loss of bulk carbon from the M35 HSS which resulted in a poor hardening response in VHT due to a lower (> ~0.9 wt. % c) carbon content. This CO was attributed to dissociation of the primary carbides above ~800 ℃ in agreement with sample mass reduction measured by TG. With the surface oxide removed, the hardening response in VHT was re-established as was the bulk carbon content.

Having the conditions necessary for optimal hardening response of HSS in VHT, chapter 4 described an industrially applicable method for improving the performance of standard HSS twist drills. Performance was characterised by material removal rate in accelerated drill testing and was achieved by using a duplex treatment incorporating plasma nitriding and PVD (with a single cycle process in a commercial chamber used to nitride and PVD coat HSS drills).

5.5 Key areas of novelty

Three areas of novelty in this research warrant separate discussion. The first area was the identification of surface oxide as a critical performance limiting feature on small diameter HSS cutting tool blanks subjected to VHT. The second area was the measurement of CO using EGA during a VHT cycle of HSS with a surface oxide. Finally, the implementation of duplex treatment in a large commercial chamber within a single process is a significant step in establishing the suitability of this method for industrial scale production.

5.5.1 Surface oxide on HSS and its effect in VHT

Critical to the performance of cutting tools is the hardening response of HSS in VHT. A correlation between surface oxide thickness and loss of carbon in VHT was established resulting in reduced performance shown in accelerated drill testing. Time at temperatures above ~800 ℃ in VHT is substantially longer than eutectic salt bath heat treatment and would explain why this loss of carbon has not been reported previously.

5.5.2 Evolution of Carbon in VHT

Evolution of CO is well known however not previously reported using EGA during VHT. Interestingly the Tc or Curie Temperature where the transition from ferromagnetic to paramagnetic was observed as was the endothermic process of dissolution of primary carbides. The coupled EGA allowed the observation of CO being evolved and agreed with the dissolution of these primary carbides which released carbon into the substrate.

5.5.3 Duplex coating as a single cycle in a commercial chamber

The central plasma employed in the large commercial chamber meant a low substrate voltage-bias at low pressure could be employed. This meant plasma nitriding operation parameters were similar to coating enabling the process to step into coating as a single process. The significance of this is that a duplex treatment could be completed without breaking vacuum. The two advantages are that there is no introduction of contaminants between processes and that it established the suitability of this method for industrial scale production.

5.6 Implications for the wider research field

It is important to view the results in the context of the wider research field and assess the value of findings to other researchers working in similar areas. In an effort to establish the value of the research presented here several points of interest will be examined.

The role of a surface oxide in VHT of HSS is of significant importance given that there is a continued move from salt to vacuum for heat treatment of HSS. The research here proves that carbon is lost

during VHT of HSS by a reduction of the surface oxide and evolution of as CO species. This evolution of CO coincides with dissolution of primary carbides.

Commercial plasma nitriding is usually conducted using direct current (DC) glow discharge bias voltages significantly higher with the resultant problems of edge effect and hollow cathode effect. The use of a central plasma in this research is of significant importance to the wider field since to date, research has often concerned plasma assisted DC glow discharge. The central plasma allows an independent voltage bias on the HSS tools, alleviating hollow cathode and edge effects. Importantly, process conditions are similar to those required for PVD coating, making the adoption of duplex coatings commercially viable.

This work adds to the wider field since it builds on previous research into functionally graded coatings, interrupted coatings, metallic interlayers and lattice mismatch between coating and substrate and the importance of better substrate support to reduce plastic deformation. Duplex processes usually involve separate chambers for plasma nitriding and PVD coating. Breaking vacuum and changing chambers introduces contaminants such as dust and oxygen which affect the adhesion of the PVD coating. There is also the commercial cost compared to a single chamber.

Chapter 6. Conclusion

The primary aims of this research project have been met. The first primary aim was to elucidate mechanisms for observed variations in the hardness of VHT HSS tools. Surface oxide was found to be critical in determining the hardness of VHT HSS drills less than 5 mm in diameter. Carbon released into the HSS material bulk during dissociation of the primary carbides readily combined with the oxygen in the scale and was evolved as CO. Removal of the scale prevented this occurring and full hardness was achieved. A link between carbon content and hardening response in VHT was established. The role of the surface oxide in VHT of HSS was observed with an almost linear relationship between carbon content and hardness response in VHT shown with incremental removal of surface oxide. The surface oxide reduces above ~ 800 ℃ when the dissolution of primary carbides

releasing carbon into the HSS substrate which readily combines with oxygen in the surface oxide and evolves as CO, measured by EGA which was associated with sample mass loss.

Improving the performance of HSS drills was the second primary aim and was achieved using a duplex treatment performed for the first time in an industrial scale system. The tool life was greatly extended due to reduced substrate deformation during operation. Excellent adhesion between the coating and nitrided substrate was mandatory and was achieved using single cycle operation (with no contamination introduced through transfer) and reduced nitriding substrate bias, enabled due to the central plasma in the INNOVA coating system. As expected with this duplex treatment, a lack of substrate deformation resulted in prolonged tool life. This benefit would be offset if coating adhesion were not excellent. The Innova features a central plasma for ion bombardment of the surface which prepares the surface for plasma nitriding and for PVD coating which contributes to this excellent adhesion and the ability to perform duplex treatment in this system without breaking vacuum is also significant in minimising surface contaminants for maximising adhesion to the substrate.

6.1 Further work

There are several avenues for further work which could aid the understanding of carbon loss in VHT of HSS and provide improved performance in duplex coated HSS tools. High strain deformation from cold drawing of HSS appears to have an effect on the loss of carbon in VHT. While this effect was less significant than effects due to surface oxide, it is still worthy of further investigation. Fractured primary carbides, larger than 5 μm, were observed in this research and occurred after cold drawing of the HSS. Micro-voids which accompany fractured carbides have been observed within drawn HSS [7]. The authors stated that these micro-voids contributed to lower measured hardness after VHT. These fractured carbides/micro-voids are considered to be a secondary mechanism for reduced hardness following VHT but could be influential particularly if they occur in close proximity to the cutting edge of HSS tools.

While research into species evolved with respect to distance from the plasma has been conducted, the nitriding response with respect to distance from the central plasma during nitriding could be investigated in more detail. The conditions used for nitriding in this research (central plasma with low pressure and low voltage-bias) reduced edge- and hollow cathode- effects and this aspect deserves further investigation. Finally, the benefits of duplex coating could be extended with functionally graded and/or multilayer or interrupted coatings.

Bibliography

1. Bollier, R. *World Cutting and Machine Tool Markets*. in *Advanced Materials Conference*. 1999. Florida, USA.
2. Taylor, F.W., *On the art of cutting metals.* 1907.
3. Doyle, E.D., *Effect of different heat treatments on the wear of high speed steel cutting tools.* Wear, 1974. **27**(3): p. 295-301.
4. Söderberg, S., O. Vingsbo, and M. Nissle, *Performance and failure of high speed steel drills related to wear.* Wear, 1982. **75**(1): p. 123-143.
5. Zong, J. and J. Yoon, *Theoretical interpretation of the decarburization mechanism in convective oxygen steelmaking.* Metallurgical and Materials Transactions B, 1990. **21**(1): p. 49-57.
6. Wisell, H., *New Developments in High Speed Steel*, in *International Federation of Heat Treatment and Surface Engineering*. 2000.
7. Yanagisawa, T., et al., *The Effect of Cold Drawing on the Hardening and Tempering Hardness of Tool Steels.* Denki Seiko (Electr. Furn. Steel), 1986. **57**(3): p. 170-180.
8. Griffith, A.A., *The phenomena of rupture and flow in solids.* Philosophical transactions of the royal society of london. Series A, containing papers of a mathematical or physical character, 1921: p. 163-198.
9. Ko, D.-C. and B.-M. Kim, *The prediction of central burst defects in extrusion and wire drawing.* Journal of Materials Processing Technology, 2000. **102**(1–3): p. 19-24.
10. Teimer, D.A., A.G. Petrenko, and L.A. Kurtova, *Prevention of decarburization in the annealing of high-speed steel.* Metal Science and Heat Treatment, 1960. **2**(5): p. 269-272.
11. Chen, Y., et al., *On the formation of vacancies in alpha -ferrite of a heavily cold-drawn pearlitic steel wire.* Scripta Materialia, 2011. **64**(5): p. 390-393.
12. Atienza, J.M. and M. Elices, *Influence of residual stresses in the tensile test of cold drawn wires.* Materials and Structures, 2003. **36**(262): p. 548-548-552.
13. Toribio, J. and E. Ovejero, *Effect of Cold Drawing on Microstructure and Corrosion Performance of High-Strength Steel.* Mechanics of Time-Dependent Materials, 1997. **1**(3): p. 307-319.
14. Brandt, D.A. and J.C. Warner, *Metallurgy fundamentals*. 1999: Goodheart-Willcox.
15. Trent, E.M. and P.K. Wright, *Metal Cutting*. Materials & Mechanical. 2000: Butterworth-Heinemann. 1-464.
16. Jones, B. and W. Sleepers, *Technology and the Future of Work.* Brighton: Wheatsheaf Books, 1982.
17. Day, C., *The Taylor-White process of treating tool steel, and its influence on the mechanic arts.* Journal of the Franklin Institute, 1901. **152**(3): p. 161-178.
18. Roberts, G.A. and R. Kennedy, *Tool steels*. 1998: ASM International.
19. Honeycombe, R.W.K., ed. *Steels--Microstructure and Properties*. 1981, Edward Arnold Ltd , 41 Bedford Square, London, WC1B 3DQ, England.
20. Fischmeister, H.F., S. Karagoz, and H.O. Andren, *An Atom Probe Study of Secondary Hardening in High Speed Steels.* Acta Metall., 1988. **36**(4): p. 817-825.
21. Hirth, J., E. Dulis, and V. Chandhok, *The Contribution of Cobalt to the Tempering Resistance and Hot Hardness of Tool Steels and Cobalt Replacement.* Strength of Metals and Alloys, 1982. **1**: p. 185-191.
22. Rong, W., et al., *The role of alloy composition in the precipitation behaviour of high speed steels.* Acta Metallurgica et Materialia, 1992. **40**(7): p. 1727-1738.
23. Kayser, F. and M. Cohen, *Carbides in high-speed steel-Their nature and quantity.* Metal Progress, 1952. **61**(6): p. 79-85.
24. Malkiewicz, T., Z. Bojarski, and J. Foryst, *Carbides in Annealed and Quenched High Speed Steels.* J. Iron Steel Inst, 1959. **193**: p. 25.
25. Goldschmidt, H., *A High-Temperature X-Ray Study on High-Speed Steel.* J. Iron & Steel Inst, 1957. **186**: p. 68.
26. Hoyle G, ed. *High Speed Steel*. 1988, Butterworths: Cambridge 1988.

27. Brust, S., *Transformation of Surface Oxides during Vacuum Heat Treatment of a Powder Metallurgical Hot Work Tool Steel*, in *Department of Materials and Manufacturing Technology*. 2013, Chalmers University of Technology: Gothenburg.
28. Kuo, K., *Carbide Precipitation, Secondary Hardening and Red Hardness of High Speed Steel*. Journal of the Iron and Steel Institute, 1953. **223**.
29. Fischmeister, H., R. Riedl, and S. Karagöz, *Solidification of high-speed tool steels.* Metallurgical Transactions A, 1989. **20**(10): p. 2133-2148.
30. Serna, M.M. and J.L. Rossi, *MC complex carbide in AISI M2 high-speed steel.* Materials Letters, 2009. **63**(8): p. 691-693.
31. Xie, C., et al., *Inheritance of Precipitated V sub 4 C sub 3 in Martensitic Transformation.* Acta Metallurgica Sinica (China) (Peoples Republic of China), 1991. **27**(5): p. A330-A336.
32. Bocanegra-Bernal, M.H., *Hot Isostatic Pressing (HIP) technology and its applications to metals and ceramics.* Journal of Materials Science, 2004. **39**(21): p. 6399-6420.
33. Bell, T., *Sub-atmospheric pressure or vacuum heat-treatment processing.* Metals Technology, 1974. **1**(1): p. 209-221.
34. Doyle, E.D., J.G. Horne, and D. Tabor, *Frictional interactions between chip and rake face in continuous chip formation.* Proceedings of the Royal Society of London, Series A (Mathematical and Physical Sciences), 1979. **366**(1725): p. 173-83.
35. Olsson, M. and S. Hogmark, *Wear mechanisms of HSS cutting tools.* Gear Solutions, 2008: p. 20-29.
36. Söderberg, S. and S. Hogmark, *Wear mechanisms and tool life of high speed steels related to microstructure.* Wear, 1986. **110**(3–4): p. 315-329.
37. Dexter, G. *Salt bath vs. vacuum furnace hardening of M 2 high speed and D 2 tool steel*. in *Heat Treating. Proceedings of the 16 th Conference*. 1996.
38. Lyapunov, A.I., *Heat treatment of tools in vacuum.* Metal Science and Heat Treatment (Russia) (USA), 2001. **43**(11-12): p. 429-429-430.
39. Leskovsek, V. and B. Ule, *Improved vacuum heat-treatment for fine-blanking tools from high-speed steel M2.* Journal of Materials Processing Technology, 1998. **82**(1-3): p. 89-94.
40. Leskovšek, V., B. Šuštaršič, and G. Jutriša, *The influence of austenitizing and tempering temperature on the hardness and fracture toughness of hot-worked H11 tool steel.* Journal of Materials Processing Technology, 2006. **178**(1): p. 328-334.
41. Belinato, G., L.C. Canale, and G.E. Totten, *Gas Quenching.* Quenching Theory and Technology, 2010: p. 445.
42. Doehaerd, T., P. Goldfinger, and F. Waelbroeck, *Direct determination of the sublimation energy of carbon.* The Journal of Chemical Physics, 1952. **20**(4): p. 757-757.
43. Hoch, M., et al., *The Heat of Sublimation of Carbon.* The Journal of Physical Chemistry, 1955. **59**(2): p. 97-99.
44. Marshall, A. and F. Norton, *Carbon vapor pressure and heat of vaporization.* Journal of the American Chemical Society, 1950. **72**(5): p. 2166-2171.
45. Gonçalves, C.S., et al., *Effect of cooling rate during quenching on the toughness of high speed steels.* Journal of ASTM International, 2011. **8**(4).
46. Rong, W. and G.L. Dunlop, *The crystallography of secondary carbide precipitation in high speed steel.* Acta Metallurgica, 1984. **32**(10): p. 1591-1599.
47. Leitner, H., et al., *Analysis of the precipitation behaviour in a high-speed steel by means of small-angle neutron scattering.* Materials Science and Engineering A, 2005. **398**(1-2): p. 323-331.
48. Versaci, R.A., *Stability of carbides in M2 high speed steel.* Journal of Materials Science Letters, 1988. **7**(3): p. 273-275.
49. Yu, T., C. Chen, and J. Yang, *Decomposition of Retained Austenite in a High-Speed Steel GPM A30.* Journal of Materials Engineering and Performance, 2007. **16**(1): p. 102-108.
50. Karagöz, S., et al., *Microstructural changes during overtempering of high-speed steels.* Metallurgical Transactions A, 1992. **23**(6): p. 1631-1640.
51. Zhu, Q., et al., *Three dimensional microstructure study of oxide scale formed on a high-speed steel by means of SEM, FIB and TEM.* Corrosion Science, 2011. **53**(11): p. 3603-3611.

52. Molinari, A., et al., *Primary Carbides in spincast HSS for hot rolls and their effect on the oxidation behaviour.* 2002.
53. Bramley, A. and K. Allen, *The Loss of Carbon from Iron and Steel when Heated in Decarburizing Gases.* Engineering, 1932. **133**: p. 92-94.
54. Sachs, K. and C. Tuck, *Surface oxidation of steel in industrial furnaces.* J. Iron Steel Inst 1968. **111**: p. 1-17.
55. Chen, R.Y. and W.Y.D. Yuen, *Oxide-scale structures formed on commercial hot-rolled steel strip and their formation mechanisms.* Oxidation of Metals (USA), 2001. **56**(1-2): p. 89-118.
56. Molinari, A., et al., *Influence of microstructure and chromium content on oxidation behaviour of spin cast high speed steels.* Materials Science and Technology, 2001. **17**(4): p. 425-425.
57. Baud, J., et al., *The oxidation and decarburizing of Fe-C alloys in air and the influence of relative humidity.* Oxidation of Metals, 1975. **9**(1): p. 69-97.
58. Stout, R. and T. Aho, *Surface Effects Accompanying the Heating of Carbon Tool Steel in Oxidizing Atmospheres.* Controlled Atmospheres, 1942.
59. Leprince, G., et al., *Experimental study and modelling of oxidation-decarburization phenomena in spring steels.* Revue de Metallurgie-Cahiers d Informations Techniques, 1999. **96**(10): p. 1275-1287.
60. Fruehan, R., *The rate of reduction of iron oxides by carbon.* Metallurgical Transactions B, 1977. **8**(1): p. 279-286.
61. Jozwiak, W.K., et al., *Reduction behavior of iron oxides in hydrogen and carbon monoxide atmospheres.* Applied Catalysis A: General, 2007. **326**(1): p. 17-27.
62. Srinivasan, N. and A. Lahiri, *On the mechanism of iron oxide reduction by carbon.* Metallurgical Transactions B, 1975. **6**(2): p. 269-274.
63. Caplan, D., et al., *Oxidation of Fe-C alloys at 500° C.* Oxidation of Metals, 1978. **12**(1): p. 67-82.
64. Mondal, K., et al., *Reduction of iron oxide in carbon monoxide atmosphere—reaction controlled kinetics.* Fuel Processing Technology, 2004. **86**(1): p. 33-47.
65. Mayott, S.W., *Analysis of the Effects of Reduced Oxygen Atmospheres on the Decarburization Depths of 300M Alloy Steel*. 2010, Rensselaer Polytechnic Institute.
66. Kogan, Y.D., *A brief historical review.* Metal Science and Heat Treatment, 1974. **16**(3): p. 197-199.
67. Pye, D., *Practical Nitriding and Ferritic Nitrocarburizing*. first ed. Practical Nitriding and Ferritic Nitrocarburizing, ed. D. Pye. 2003: ASM International, Materials Park, OH, 44073-0002, USA. 256-256.
68. Pessin, M.A., et al., *The effects of plasma nitriding process parameters on the wear characteristics of AISI M2 tool steel.* Tribology Letters (Netherlands), 2000. **8**(4): p. 223-228.
69. Podgornik, B., et al., *Improving tribological properties of tool steels through combination of deep-cryogenic treatment and plasma nitriding.* Wear, 2012. **288**(0): p. 88-93.
70. Cahn, R. and P. Haasen, *Physical Metallurgy, 4th revised and enhanced ed., 3 vols*. 1996, North-Holland, Amsterdam.
71. Bell, T., *Ferritic Nitrocarburising.* Heat Treatment of Metals, 1975. **2**(2): p. 39-49.
72. Georges, J., *Nitriding process and nitriding furnace therefor*. 1999, Google Patents.
73. B. Berghaus, G.P., DPR, 668,532 (1932). *DPR, 668,532*. 1932.
74. B. Berghaus, G.P., DPR, 851,560 (1939).
75. Yurgenson, A., *Development of nitriding.* Metal Science and Heat Treatment, 1968. **9**(7): p. 485-491.
76. Figueroa, C.A. and F. Alvarez, *On the hydrogen etching mechanism in plasma nitriding of metals.* Applied Surface Science, 2006. **253**(4): p. 1806-1809.
77. Hubbard, P., *Characterisation of a commercial active screen plasma nitriding system.* 2007.
78. Muratore, C., et al., *Low-temperature nitriding of stainless steel in an electron beam generated plasma.* Surface and Coatings Technology, 2005. **191**(2–3): p. 255-262.
79. Muratore, C., et al., *Effect of plasma flux composition on the nitriding rate of stainless steel.* Journal of Vacuum Science & Technology A: Vacuum, Surfaces, and Films, 2004. **22**(4): p. 1530-1535.

80. Wei, R., *Low energy, high current density ion implantation of materials at elevated temperatures for tribological applications.* Surface and Coatings Technology, 1996. **83**(1–3): p. 218-227.
81. Figueroa, C., E. Ochoa, and F. Alvarez, *Influence of the ion mean free path and the role of oxygen in nitriding processes.* Journal of applied physics, 2003. **94**(4): p. 2242-2247.
82. Janosi, S., Z. Kolozsvary, and A. Kis, *Controlled hollow cathode effect: new possibilities for heating low-pressure furnaces.* Metal Science and Heat Treatment, 2004. **46**(7-8): p. 310-316.
83. Li, C.X., *Active screen plasma nitriding - an overview.* Surface Engineering, 2010. **26**(1-2): p. 135-141.
84. Corujeira Gallo, S. and H. Dong, *On the fundamental mechanisms of active screen plasma nitriding.* Vacuum, 2009. **84**(2): p. 321-325.
85. Zhao, C., et al., *Study on the active screen plasma nitriding and its nitriding mechanism.* Surface and Coatings Technology, 2006. **201**(6): p. 2320-2325.
86. Kwietniewski, C., et al., *Nitrided layer embrittlement due to edge effect on duplex treated AISI M2 high-speed steel.* Surface and Coatings Technology, 2004. **179**(1): p. 27-32.
87. Nayal, G., et al., *Influence of sample geometry on the effect of pulse plasma nitriding of M2 steel.* Surface and Coatings Technology, 1999. **111**(2): p. 148-157.
88. Saikia, P., et al., *Role of substrate and deposition conditions on the texture evolution of titanium nitride thin film on bare and plasma-nitrided high-speed steel.* Journal of Theoretical and Applied Physics, 2013. **7**(1): p. 1-12.
89. Nickel, J., et al., *Evaluation of the wear of plasma-nitrided and TiN-coated HSS drills using conventional and micro-PIXE techniques.* Wear (Switzerland), 2000. **239**(2): p. 155-167.
90. Mahboubi, F. and M. Fattah, *Duplex treatment of plasma nitriding and plasma oxidation of plain carbon steel.* Vacuum, 2005. **79**(1–2): p. 1-6.
91. Huang, H.H., J.L. He, and M.H. Hon, *Microstructure and mechanical properties of surface layer obtained by plasma nitriding and/or TiN coating on high speed steel.* Surface and Coatings Technology, 1994. **64**(1): p. 41-46.
92. Kadlec, J., V. Hrubý, and M. Novak, *Influencing properties of high-speed cutting steel, ion-nitrided and subsequently coated.* Vacuum, 1990. **41**(7): p. 2226-2229.
93. Nishimoto, A., et al., *Simultaneous duplex process of TiN coating and nitriding by active screen plasma nitriding.* Surface and Coatings Technology, 2012. **228**: p. S558–S562.
94. Doyle, E.D., et al., *Nitriding of high speed steel.* International Heat Treatment and Surface Engineering, 2011. **5**(2): p. 69-72.
95. da Silva Rocha, A., et al., *Microstructure and residual stresses of a plasma-nitrided M2 tool steel.* Surface and Coatings Technology, 1999. **115**(1): p. 24-31.
96. Li, C.X. and T. Bell, *A comparative study of low temperature plasma nitriding, carburising and nitrocarburising of AISI 410 martensitic stainless steel.* Materials Science and Technology, 2007. **23**(3): p. 355-361.
97. Leonhardt, D., C. Muratore, and S.G. Walton, *Applications of electron-beam generated plasmas to materials processing.* IEEE Transactions on Plasma Science, 2005. **33**(2): p. 783-90.
98. Matthews, A. and A. Leyland, *Widening the market for advanced PVD coatings.* Journal of Materials Processing Technology, 1996. **56**(1): p. 757-764.
99. Bunshah, R. and A. Raghuram, *Activated reactive evaporation process for high rate deposition of compounds.* Journal of Vacuum Science and Technology, 1972. **9**(6): p. 1385-1388.
100. Anders, A., *The evolution of ion charge states in cathodic vacuum arc plasmas: A review.* Plasma Sources Science and Technology, 2012. **21**(3).
101. Vogel, J., *Ion plating processes of wear resistant coatings on tools*. 1989, Chichester, UK: Ellis Horwood Ltd. p. 165-196.
102. Anders, A., *Approaches to rid cathodic arc plasmas of macro-and nanoparticles: a review.* Surface and Coatings Technology, 1999. **120**: p. 319-330.
103. Martin, P., et al., *Characteristics of titanium arc evaporation processes.* Thin Solid Films, 1987. **153**(1): p. 91-102.

104. Knotek, O., et al. *Hard coatings for cutting and forming tools by PVD arc processes*. in *Materials Science Forum*. 1997: Trans Tech Publ.
105. Matthews, A. and V. Murawa, *Latest work with TiN coatings extends tool life.* Chart. Mech. Eng., 1985. **32**(10): p. 31-34.
106. Feinberg, B., *Longer Life from TiN Tools.* MFG Eng. Manage, 1971. **67**(1): p. 16-18.
107. Bendavid, A., et al., *The properties of TiN films deposited by filtered arc evaporation.* Surface and Coatings Technology, 1994. **70**(1): p. 97-106.
108. Münz, W.D., *Titanium aluminum nitride films: A new alternative to TiN coatings.* Journal of Vacuum Science & Technology A, 1986. **4**(6): p. 2717-2725.
109. Lai, F. and J. Wu, *Structure, hardness and adhesion properties of CrN films deposited on nitrided and nitrocarburized SKD 61 tool steels.* Surface and Coatings Technology, 1997. **88**(1): p. 183-189.
110. Fox-Rabinovich, G., et al., *Effect of mechanical properties measured at room and elevated temperatures on the wear resistance of cutting tools with TiAlN and AlCrN coatings.* Surface and Coatings Technology, 2006. **200**(20): p. 5738-5742.
111. Bemporad, E., et al., *Characterization and hardness modelling of alternate TIN/TICN multilayer cathodic arc PVD coating on tool steel.* Surface and Coatings Technology, 2001. **146**: p. 363-370.
112. Jindal, P.C., D.T. Quinto, and G.J. Wolfe, *Adhesion measurements of chemically vapor deposited and physically vapor deposited hard coatings on WC-Co substrates.* Thin Solid Films, 1987. **154**(1–2): p. 361-375.
113. Mitterer, C., P. Mayrhofer, and J. Musil, *Thermal stability of PVD hard coatings.* Vacuum, 2003. **71**(1): p. 279-284.
114. Gunnars, J. and U. Wiklund, *Determination of growth-induced strain and thermo-elastic properties of coatings by curvature measurements.* Materials Science and Engineering: A, 2002. **336**(1–2): p. 7-21.
115. Castanho, J.M. and M.T. Vieira. *Laminated composite thin films: a solution to improve cutting tools performance*. in *Materials Science Forum*. 2006: Trans Tech Publ.
116. PalDey, S. and S. Deevi, *Single layer and multilayer wear resistant coatings of (Ti, Al) N: a review.* Materials Science and Engineering: A, 2003. **342**(1): p. 58-79.
117. Leyland, A. and A. Matthews, *Design criteria for wear-resistant nanostructured and glassy-metal coatings.* Surface and Coatings Technology, 2004. **177**: p. 317-324.
118. Lii, D.-F., J.-L. Huang, and M.-H. Lin, *The effects of TiAl interlayer on PVD TiA1N films.* Surface and Coatings Technology, 1998. **99**(1): p. 197-202.
119. Matthews, A., R. Jones, and S. Dowey, *Modelling the deformation behaviour of multilayer coatings.* Tribology Letters, 2001. **11**(2): p. 103-106.
120. Sinkovits, T., et al., *X-ray diffraction stress analysis of interrupted titanium nitride films: Combining the sin 2 ψ and crystallite group methods.* Thin Solid Films, 2014. **562**: p. 206-210.
121. Bell, T., H. Dong, and Y. Sun, *Realising the potential of duplex surface engineering.* Tribology International, 1998. **31**(1): p. 127-137.
122. Rousseau, A., et al., *Microstructural and tribological characterisation of a nitriding/TiAlN PVD coating duplex treatment applied to M2 High Speed Steel tools.* Surface and Coatings Technology, 2015. **272**: p. 403-408.
123. Podgornik, B., et al., *Wear and friction behaviour of duplex-treated AISI 4140 steel.* Surface and Coatings Technology, 1999. **120–121**(0): p. 502-508.
124. Yang, S., et al., *Development of advanced duplex surface systems by combining CrAlN multilayer coatings with plasma nitrided steel substrates.* Surface and Coatings Technology, 2013. **236**: p. 2-7.
125. Sanchette, F., et al., *Single cycle plasma nitriding and hard coating deposition in a cathodic arc evaporation device.* Surface and Coatings Technology, 1997. **94–95**(0): p. 261-267.
126. Sato, T., et al., *Development of a hybrid coating process as an advanced surface modification for cutting tools and moulds.* Surface and Coatings Technology, 2003. **169**: p. 45-48.
127. (CEN), *EN ISO 9556:1989 Steel and Iron - Determination of total carbon content*, in *Infrared absorption method after combustion in an induction furnace*. 2001, CEN: Brussels. p. 2-11.

128. Test, D.-B.A., *Verein Deutscher Ingenieure (VDI).* Richlinie, 1992. **3198**: p. 7.
129. Rousseau, A., E. Doyle, and D. McCulloch, *Vacuum heat treatment of high speed steel cutting tools.* International Heat Treatment & Surface Engineering, 2013. **7**(3): p. 110-114.
130. Rousseau, A.F., et al., *Carbon Evolution during Vacuum Heat Treatment of High Speed Steel.* Vacuum.
131. Stanley, J., *Steel Carburization and Decarburization–A Theoretical Analysis.* Iron Age, 1943. **151**: p. 31-35.
132. Wengcheng, L.D.X.G.L. and L. Xin, *Carbides in cold drawn wire of High Speed Steel [J].* Gangtie, 1988. **9**: p. 007.
133. McFarlane, J. and D. Tabor, *Relation between friction and adhesion.* Proceedings of the Royal Society of London. Series A. Mathematical and Physical Sciences, 1950. **202**(1069): p. 244-253.